4(1*H*)-quinolone derivatives overcome acquired resistance to anti-microtubule agents by targeting the colchicine site of β-tubulin

Ming-Shiu Lin, Tse-Ming Hong, Ting-Hung Chou, Shuenn-Chen Yang, Wei-Chia Chung, Chia-Wei Weng, Mei-Ling Tsai, Ting-Jen Rachel Cheng, Jeremy J.W. Chen, Te-Chang Lee, Chi-Huey Wong, Rong-Jie Chein, Pan-Chyr Yang

PII: S0223-5234(19)30718-4

DOI: https://doi.org/10.1016/j.ejmech.2019.111584

Reference: EJMECH 111584

To appear in: *European Journal of Medicinal Chemistry*

Received Date: 14 June 2019

Revised Date: 30 July 2019

Accepted Date: 1 August 2019

Please cite this article as: M.-S. Lin, T.-M. Hong, T.-H. Chou, S.-C. Yang, W.-C. Chung, C.-W. Weng, M.-L. Tsai, T.-J. Rachel Cheng, J.J.W. Chen, T.-C. Lee, C.-H. Wong, R.-J. Chein, P.-C. Yang, 4(1*H*)-quinolone derivatives overcome acquired resistance to anti-microtubule agents by targeting the colchicine site of β-tubulin, *European Journal of Medicinal Chemistry* (2019), doi: https://doi.org/10.1016/j.ejmech.2019.111584.

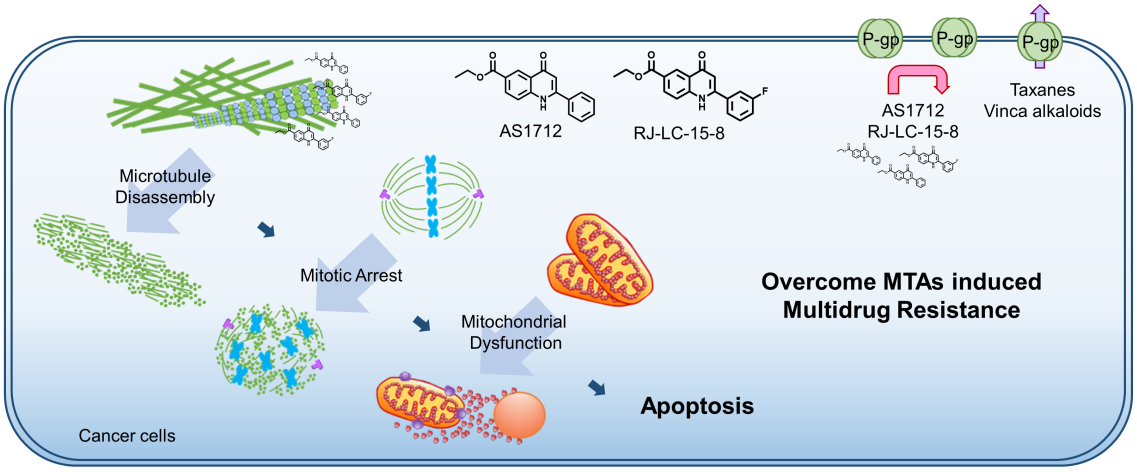

4(1*H*)-Quinolone Derivatives Overcome Acquired Resistance to Anti-microtubule Agents by Targeting the Colchicine Site of β-Tubulin

Ming-Shiu Lin[1, 2], Tse-Ming Hong[3], Ting-Hung Chou[4], Shuenn-Chen Yang[2], Wei-Chia Chung[2], Chia-Wei Weng[5], Mei-Ling Tsai[4], Ting-Jen Rachel Cheng[6], Jeremy J. W. Chen[5], Te-Chang Lee[1, 2], Chi-Huey Wong[6], Rong-Jie Chein[4, *], and Pan-Chyr Yang[1, 2, 7, *]

[1]Program in Molecular Medicine, National Yang-Ming University and Academia Sinica, Taipei, Taiwan

[2]Institute of Biomedical Sciences, Academia Sinica, Taipei 115, Taiwan

[3]Institute of Clinical Medicine, National Cheng Kung University, Tainan 701, Taiwan

[4]Institute of Chemistry, Academia Sinica, Taipei 115, Taiwan

[5]Institute of Biomedical Sciences, National Chung Hsing University, Taichung 402, Taiwan

[6]The Genomics Research Center, Academia Sinica, Taipei 115, Taiwan

[7]Department of Internal Medicine, College of Medicine, National Taiwan University, Taipei 100, Taiwan

*Corresponding author

E-mail addresses: pcyang@ntu.edu.tw (P.C. Yang); rjchein@chem.sinica.edu.tw (R.J. Chein)

ABSTRACT: Developing new therapeutic strategies to overcome drug resistance of cancer cells is an ongoing endeavor. From among 2 million chemicals, we identified ethyl 4-oxo-2-phenyl-1,4-dihydroquinoline-6-carboxylate (AS1712) as a low-toxicity inhibitor of lung cancer cell proliferation and xenograft tumor growth. We show that AS1712 is active against broad cancer cell lines and is able to bind in the colchicine-binding pocket of β-tubulin, thereby inhibiting microtubule assembly and, consequently, inducing mitotic arrest and apoptosis. Our cell-based structure-activity relationship study identified a new lead compound, RJ-LC-15-8, which had a greater anti-proliferative potency for H1975 cells than did AS1712, while maintaining a similar mechanism of action. Notably, AS1712 and RJ-LC-15-8 overcame P-glycoprotein efflux pump and β-tubulin alterations that lead to acquired resistance against microtubule-targeting drugs of cancer cells. AS1712 and RJ-LC-15-8 may be lead compounds that overcome acquired resistance to microtubule-targeting agents of cancer cells.

KEYWORDS: microtubule-targeting agents, acquired resistance, p-glycoprotein

Introduction

Cancer is the second most common cause of death worldwide, and lung cancer is the leading cause of cancer-related deaths [1]. Despite advances in treatment during the past 20 years, the prognosis for lung cancer patients remains poor [2]. Drug resistance limits the efficacy of anticancer agents and is responsible for treatment failure in most cases [3-5]. Consequently, the development of new drugs to overcome drug resistance and improve survival of cancer patients is urgently needed.

Microtubules are long, hollow cylinders composed of heterodimeric α/β-tubulin units. They are an important component of the cell cytoskeleton and are involved in mitosis, motility, and organelle transport [6-8]. Cancer cells depend on microtubules for mitosis and rapid division, which makes microtubules a suitable target for anticancer agents [8-10]. Nucleation of microtubules occurs at the centrosome, and, as they are highly dynamic structures that continuously assemble and disassemble, microtubule-targeting agents (MTAs) can regulate their dynamics and, consequently, cause mitotic arrest and subsequently cell apoptosis [10-12]. MTAs, i.e., taxanes, vinca alkaloids, colchicine, and laulimalide, are classified according to their mode of action and tubulin-binding site [13]. The taxanes (e.g., paclitaxel and ixabepilone) and the vinca alkaloids (e.g., vincristine and vinblastine) are the two major types of MTAs that are widely used clinically to treat many different types of malignant cancers, including those of the lung, breast, ovary, prostate, and head and neck and leukemia [14, 15]. However, cancers in most patients who have been treated for prolonged periods with MTA become acquired resistant to the treatment protocol [3, 16].

The two major mechanisms of MTA-induced resistance involve mutations in β-tubulin and ATP-binding cassette efflux transporters [17, 18]. A structurally altering mutation at a β-tubulin drug-binding site or expression of a β-tubulin isotype with an altered conformation may interfere with the interaction between an MTA and its binding site on β-tubulin, thereby causing treatment failure [19, 20]. Efflux transporters embedded in cell membranes may pump different types of anti-cancer drug from the intracellular to the extracellular space, which decreases intracellular drug accumulation [21], resulting in multidrug resistance (MDR) and making it more difficult to treat patients with cancer [22-24]. P-glycoprotein (P-gp) was the first identified ATP-binding cassette efflux pump and has been

well characterized. MDR caused by P-gp overexpression is the most common resistance mechanism known involving clinical cancer therapies [25-27], and, therefore, finding new agents that will improve patient outcomes and circumvent drug resistance remains a major and unmet need.

In this study, we performed a two-step high-throughput screening of 2 million compounds to search for novel molecules with therapeutic activity against lung cancer. Ethyl 4-oxo-2-phenyl-1,4-dihydroquinoline-6-carboxylate (AS1712) was found to have anticancer activity *in vitro* and *in vivo* and a superior therapeutic specificity for cancer instead of normal cells. We found that AS1712 inhibited the growth of various types of cancer cells, including those of the lung, prostate, ovary, breast, colon, and head and neck and leukemia. By targeting the colchicine-binding site of β-tubulin, AS1712 induced mitotic cell cycle arrest and apoptosis. Cell-based structure-activity relationship study identified a new lead compound, RJ-LC-15-8, which had a greater anti-proliferative potency and maintained a similar mechanism of action. Notably, the distinct tubulin-binding site of AS1712 and RJ-LC-15-8 circumvented resistance caused by P-gp overexpression.

Results

AS1712 Inhibited Lung Cancer Cell Proliferation *In Vitro* and *In Vivo* and Had Broad Anti-Cancer Activity

Through high-throughput screening, a library of 2 million compounds was used to evaluate anti-proliferation activities against EGFR tyrosine kinase inhibitor (TKI)-resistant lung cancer cells (H1975) at 10 μM concentration. The coefficient of variation (CV%) and Z' values of the primary screening were determined as 4.9% and 0.58, respectively. In the first screening, ~6,800 small molecules exhibited >80% growth inhibition of H1975 cells. These compounds were further screened against other eight lung cancer cells, including clinical isolates (CL25, CL83, CL97, CL100, CL141, CL152), an ATCC cell line (PC-9) and its derivative resistant clone (PC9/IR). By filtered with the criteria of IC50 $\leq$ 6 μM for all tested cells, only 232 small molecules were kept for the further study. Ethyl 4-oxo-2-phenyl-1,4-dihydroquinoline-6-carboxylate (AS1712, Figure 1A) was one of these

molecules displaying superior cytotoxic e□ects on lung cancer cells and a notable therapeutic window between cancer cells and normal cells.

We first evaluated the cytotoxic effects of AS1712 on different non-small cell lung cancer cell lines using an MTS assay and found that AS1712 induced cell death in different EGFR-status cell lines, including A549 (wild-type EGFR), CL1-0 (wild-type EGFR), PC9 (EGFR exon 19 deletion), and H1975 (T790M and L858R mutations in EGFR). The IC_{50} values for the affected cell lines ranged from 16 to 33 nM (Figure 1B), which indicated that the cytotoxic effect of AS1712 was not related to the EGFR status of lung cancer cells. Furthermore, AS1712 was relatively non-toxic against normal bronchial epithelial (NBE) and human fibroblast (HFB) cells (IC_{50} > 10 μM; Figure 1B). The colony-forming abilities of CL1-0 and H1975 cells were suppressed in a dose-dependent manner by AS1712 (Figure 1C). The aforementioned data suggested that AS1712 inhibited non-small cell lung cancer proliferation *in vitro.*

To evaluate the *in vivo* anti-tumor efficacy of AS1712, athymic BALB/c nude mice each bearing an established subcutaneous H1975 tumor were intraperitoneally injected with DMSO (control) or with 4 or 8 mg/kg AS1712, three times a week for 25 days (n = 6 per group). The tumor volume and body mass of each mouse were monitored throughout the treatment period. Treatment with AS1712 markedly reduced H1975 xenograft tumor growth compared with that found for the control group (average tumor size, 1749 ± 234.5 mm^3 for DMSO treatment; 871.3 ± 106 mm^3 for the 4 mg/kg and 587.2 ± 67 mm^3 for 8 mg/kg treatments; all measured on day 25 and both $p < 0.01$; Figures 1D and S1). The body masses and serum biochemical markers for liver and kidney functions, including ALT, AST, BUN, and Cre, were non-toxic a□ected on day 25 of the experiment (Figures S1D, E). Thus AS1712 inhibited tumor growth with low toxicity *in vivo*.

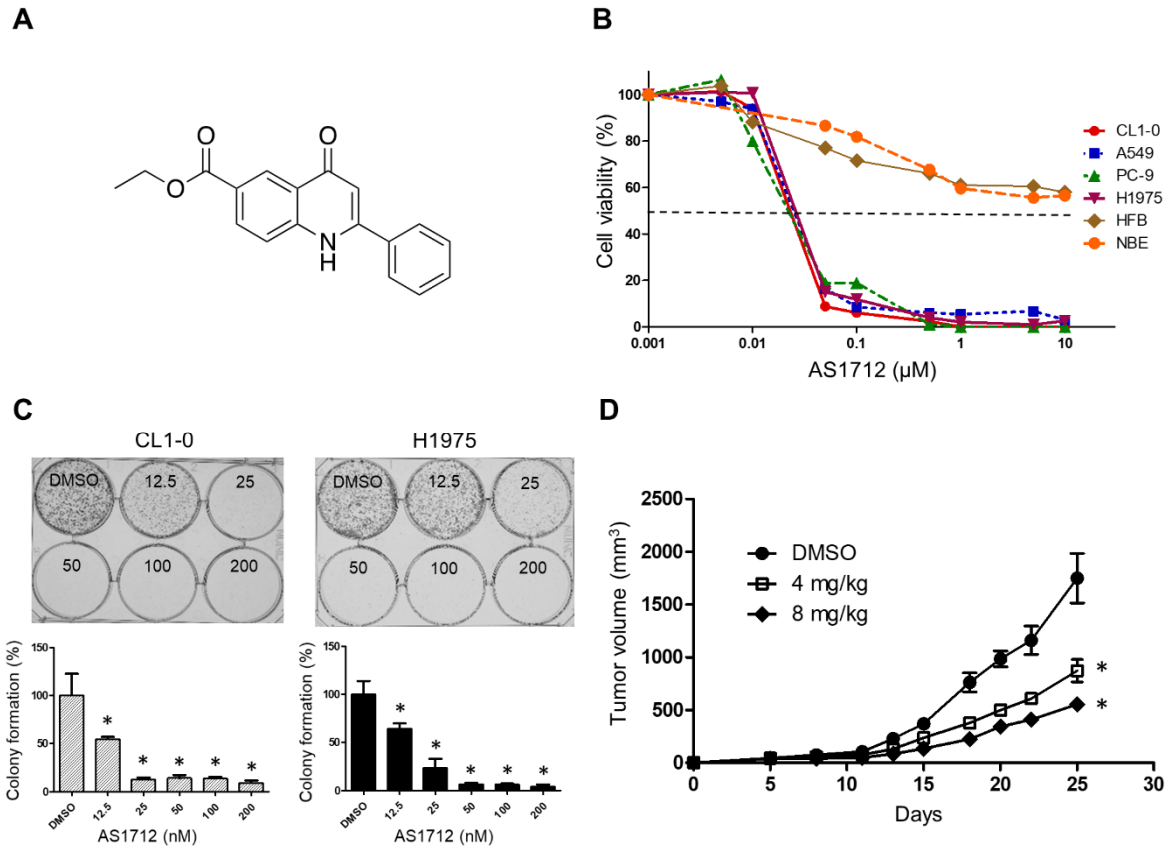

Figure 1. AS1712 inhibited cancer cell proliferation *in vitro* and *in vivo*. (A) Chemical structure of AS1712. (B) The cytotoxic effects of AS1712 on different non-small cell lung cancer and normal lung cell lines. Cells were treated with AS1712 for 72 h, and cell viability was examined by the MTS assay. Data are the mean of three determinations. (C) CL1-0 and H1975 cells were treated with AS1712 (12.5–200 nM) for 14 days. The colonies were fixed, stained with crystal violet, and then counted. Data are the mean ± SD; *$p < 0.05$. (D) H1975 cells (2×10^6) were subcutaneously injected into BALB/c nude mice. Mice were treated with DMSO or with 4 or 8 mg/kg of AS1712 intraperitoneally three times a week for the next 25 days. Tumor volumes were measured before each injection. Data are the mean ± SEM; *$p < 0.05$.

We also assessed the cytotoxicity of AS1712 against various types of cancer cells and found that AS1712 decreased the viability of many different types of malignant cells, including those derived from lung (A549, CL1-0, PC9, and H1975), breast (BT-549, Hs578t, MDA-MB-231, 37T, and 82T), ovarian (SKOV-3, IGR-OV1, and Ovcar-3), head and neck (SAS, OECM1, and KB), colon (HCT116,

HT-29, Colon205, and SW620), and prostate (Du-145 and PC-3) cancers and from leukemia (Molt4 and CCRF-CEM). For the 23 cancer cell lines tested, their IC_{50} values ranged from 16 to 84 nM (Table 1), suggesting that AS1712 or a derivative of AS1712 might be used for the treatment of various types of cancer.

Table 1. Inhibitory Activities of AS1712 against the Proliferation of different Cancer Cell lines or Normal cell lines.

Cell line	IC_{50} (nM)	Cell line	IC_{50} (nM)
Lung cancer		**Head and Neck cancer**	
A549	20 ± 0.98	SAS	78 ± 10.4
CL1-0	16 ± 2.48	OECM1	52 ± 1.94
PC9	17 ± 2.09	KB	37 ± 0.27
H1975	33 ± 4.86	**Colon cancer**	
Breast cancer		HCT116	50 ± 0.81
BT-549	33 ± 1.51	HT-29	48 ± 0.62
Hs578t	41 ± 2.87	Colon205	57 ± 5.17
MDA-MB-231	55 ± 6.83	SW620	35 ± 1.18
37T	34 ± 2.99	**Prostate cancer**	
82T	35 ± 0.67	Du-145	47 ± 1.28
Ovarian cancer		PC-3	45 ± 1.77
SKOV-3	50 ± 0.32	**Leukemia**	
IGR-OV1	84 ± 2.07	Molt4	38 ±1.03
Ovcar-3	28 ± 1.08	CCRF-CEM	45 ± 0.45
Normal cell line			
NBE	>10 μM	HFB	>10 μM

AS1712 Induced Apoptosis and Cell Cycle Arrest

To evaluate whether the cytotoxic effect of AS1712 correlated with apoptotic cell death, CL1-0, H1975, and HFB cells were treated with AS1712 for 24 to 72 h and then monitored for the activation of major pro-apoptotic proteins. We found that AS1712 induced cleavage of poly(ADP-ribose) polymerase (PARP) and caspase-3 in CL1-0 and H1975 cells in a time-dependent manner; PARP and caspase-3 in the normal HFB cells were not affected by AS1712 (Figure S2A). We then looked for apoptotic pathway proteins that might have been activated by AS1712 and found that AS1712

induced two intrinsic apoptosis pathway markers, cleavage of caspase-9 and expression of Bax, in a dose-dependent manner (Figure 2A). Conversely, the extrinsic apoptosis pathway marker, caspase-8, was not activated by AS1712 treatment (Figure 2A). We also found that a 24-h treatment with AS1712 increased the cytosolic level of cytochrome c (Figure 2B), whereas the same dose of AS1712 did not induce apoptosis in HFB cells or cytochrome c release (Figures S2B and C). AS1712 therefore induced activation of the intrinsic apoptosis pathway only in cancer cells.

Next, we explored whether the apoptotic effect of AS1712 was caused by aberrant cell cycle progression. The distribution of CL1-0, H1975, and HFB cells among phases of the cell cycle was examined by flow cytometry. AS1712 treatment increased the sub-G1 (apoptotic cell population) and the G2/M-phase population of CL1-0 and H1975 cells in a dose-dependent manner (Figure 2C) but not of HFB cells (Figure S2D). To clarify whether AS1712 induced G2 or mitotic cell cycle arrest, we characterized the cell cycle at its checkpoints for CL1-0 and H1975 cells and found that AS1712 increased the mitotic-phase markers cyclin B1 and phospho-histone H3 (p-HH3) but not the G2-phase marker cyclin A (Figure 2D). We also used high-content imaging to measure the mitosis index (the population of mitotic cells) by staining for the specific mitotic phase marker p-HH3 and found that AS1712 treatment caused CL1-0 and H1975 cells to accumulate in the mitotic phase in a dose-dependent manner (Figure 2E). Furthermore, we directly evaluated the mitotic-spindle organization using α-tubulin immunofluorescence staining and observed that arrangement of the mitotic spindles was disrupted by AS1712 treatment (Figure 2F). The aforementioned data showed that AS1712 induced mitotic cell cycle arrest.

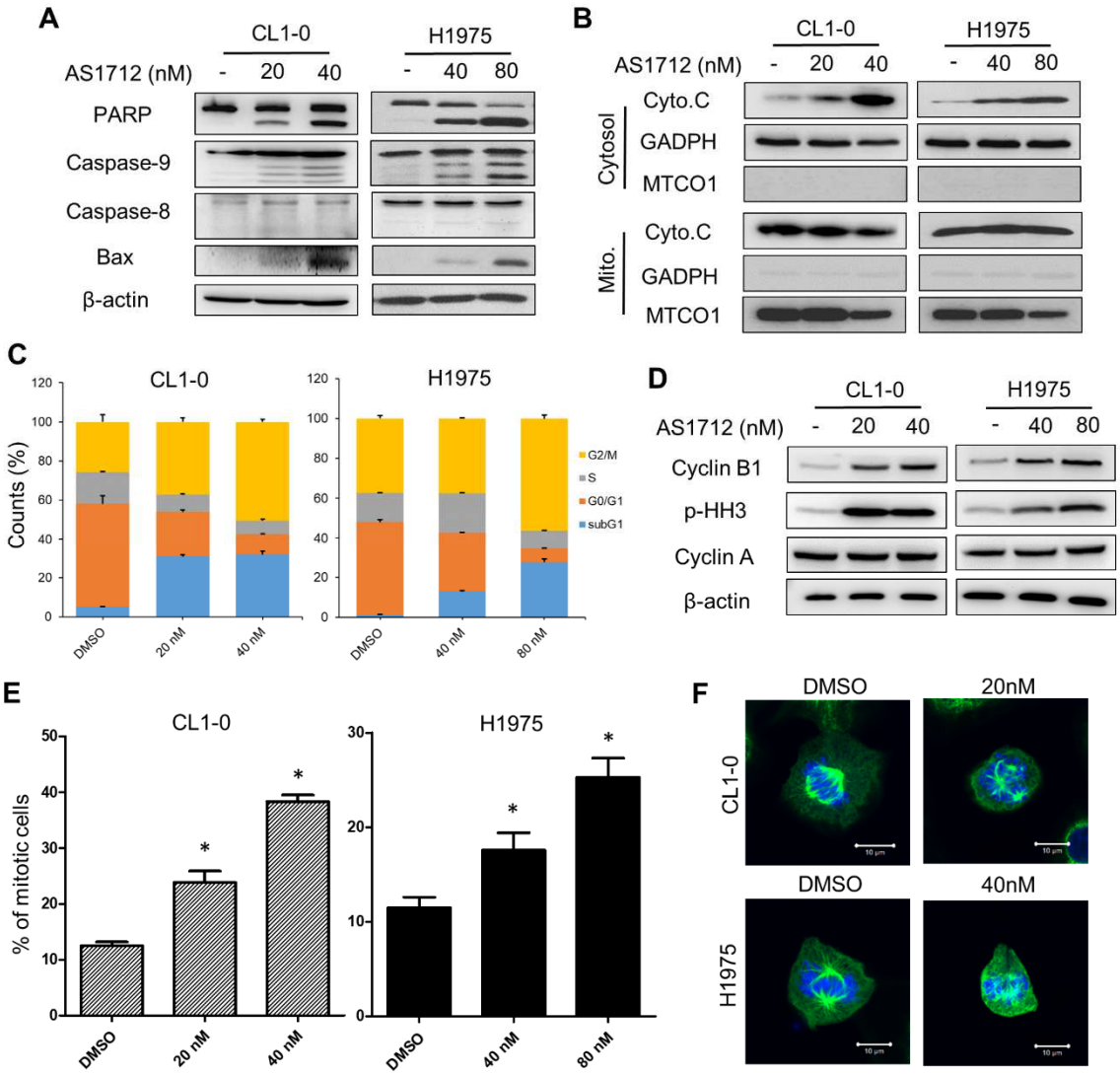

Figure 2. AS1712 induced apoptosis and cell cycle arrest in CL1-0 and H1975 lung cancer cells. Cells were treated with the indicated concentrations of AS1712 for 24 h. Then, (A) pro-apoptotic protein expression was detected by immunoblotting; (B) cytochrome c levels were assessed in the cytosolic and mitochondrial fractions; (C) cells were stained with propidium iodide to determine their DNA content by flow cytometry; (D) proteins were immunoblotted to examine their expression levels; and (E) cells were subjected to high-content imaging by p-HH3 staining to calculate the population of mitotic cells. Data are the mean ± SD; *$p < 0.05$. (F) Cells were treated with AS1712 for 6 h to observe mitotic spindle organization by α-tubulin staining (green). Immunofluorescence was detected by confocal laser microscopy. Nuclei were detected by DAPI staining (blue). Scale bar, 10 μm.

AS1712 Directly Inhibited Microtubule Polymerization

The observation that AS1712 treatment disrupted mitotic-spindle organization led us to hypothesize that the treatment might interfere with dynamic microtubule association and/or dissociation. Therefore, we performed an immunofluorescence assay to examine the status of microtubule networks in AS1712-treated CL1-0, H1975, and HFB cells. AS1712 treatment of CL1-0 and H1975 cells resulted in depolymerization of their microtubules (Figure 3A), whereas such treatment had only a minor effect on microtubules in HFB cells (Figure S2E). An in-cell microtubule assembly assay was performed, after first separating assembled and disassembled microtubules into particulate and soluble fractions, respectively, by centrifugation. Notably, AS1712 substantially increased the amount of α-tubulin in the soluble fraction, a finding similar to that found for nocodazole but not paclitaxel treatment (Figure 3B). We further confirmed that AS1712 induced depolymerization of microtubules using an immunofluorescence-based microtubule polymerization assay. H1975 cells were first treated with 40 nM AS1712 for 1 h, were then exposed to the cold for 30 min, and then were shifted to 37°C for various times. When treated with AS1712, the microtubules failed to polymerize at 37°C (Figure 3C). Next, an *in vitro* tubulin polymerization assay was used with purified tubulin to examine whether AS1712 directly interfered with microtubule assembly in a cell-free system. As expected, the reference agents nocodazole and vincristine were found to inhibit tubulin polymerization, whereas paclitaxel enhanced polymerization. AS1712 was also found to directly inhibit tubulin polymerization (Figure 3D). We also carried out an *in vitro* microtubule nucleation assay to test whether AS1712 directly inhibited the assembly of new microtubules at purified centrosomes. Purified centrosomes and tubulins were incubated with AS1712 or DMSO. AS1712 substantially inhibited the formation of microtubule asters from the centrosome (Figure 3E, left panel). A quantitative analysis of microtubule fiber length also showed a dramatic difference between AS1712 and DMSO treatments (Figure 3E, right panel). The aforementioned data showed that AS1712 directly inhibited microtubule polymerization.

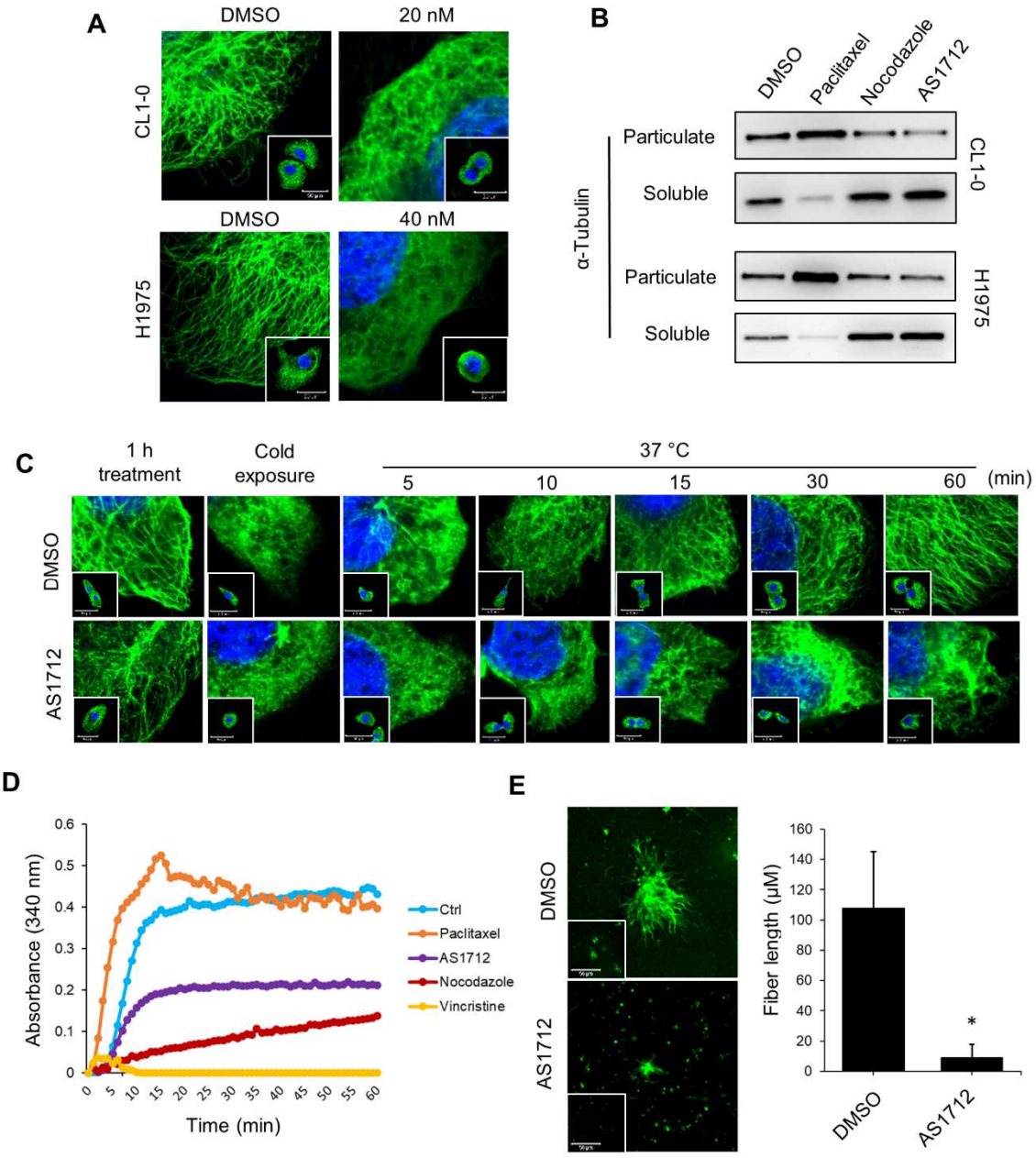

Figure 3. AS1712 inhibited microtubule polymerization. (A) Cells were incubated with AS1712 for 6-h prior to examining the microtubule networks as α-tubulin staining (green). Nuclei were detected by DAPI staining (blue). Scale bar, 50 μm. (B) Cells were incubated with DMSO, AS1712, paclitaxel, or nocodazole for 6-h and then harvested and separated into soluble (tubulin monomers) and insoluble (tubulin polymers) fractions. The amount of α-tubulin was detected by immunoblotting. (C) Immunofluorescence-based microtubule polymerization assay H1975 cells were treated with 40 nM AS1712 for 1 h, after cold exposure for 30 min, and then were incubated at 37 °C for the

indicated times. Scale bar, 50 µm. (D) Purified porcine tubulin and GTP were incubated at 37 °C with 5 µM AS1712, 5 µM paclitaxel, 5 µM vincristine, 5 µM nocodazole, or with DMSO control. Microtubule polymerization was assessed every min for 1 h by monitoring the A_{340}. (E) Purified centrosomes were first incubated with AS1712 and then with tubulin. Microtubule asters that formed were stained with monoclonal anti-α-tubulin (green). Fiber lengths were measured (n = 20 asters per group) Data are the mean ± SD. Scale bar, 50 µm.

Scheme 1. Synthesis of AS1712 analogs 2a-2m

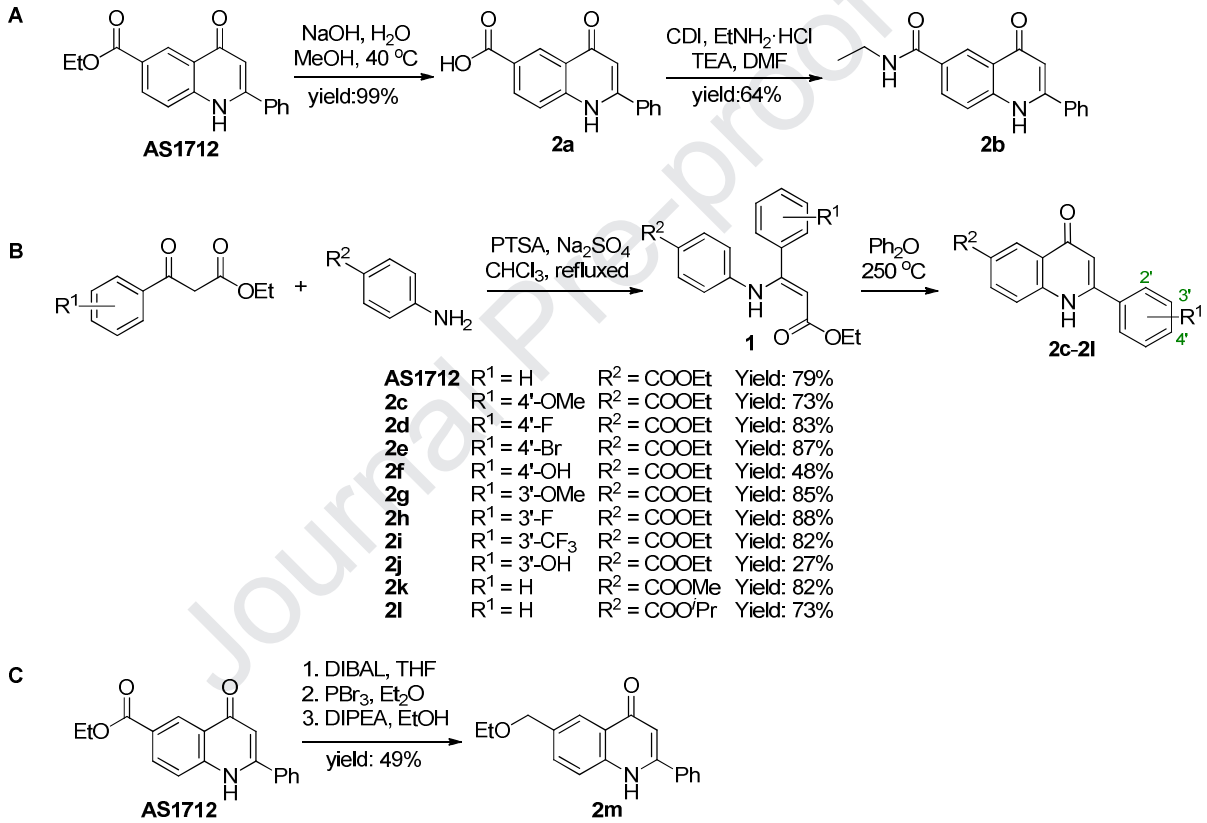

A Cell-Based Structure-Activity Relationship (SAR) Study of AS1712 Led to the Identification of the More Potent Anti-Cancer Compound RJ-LC-15-8

To find a more potent AS1712-based compound with increased anti-cancer activity, we carried out an SAR study using H1975 cells and AS1712 analogs, which possessed the 4(1*H*)-quinolone scaffold. As shown in Scheme 1A and Table 2, AS1712 was first hydrolyzed to the acid **2a**, which had an IC_{50} > 5 µM. Next **2a** was transformed into the ethyl amide **2b**, which had an IC_{50} = 3.7 µM.

Both analogs had substantially less activity against H1975 cells then did AS1712. We then focused on structural optimization of the phenyl group at the C-2 position of the 4(1*H*)-quinolone scaffold. The effects of substituents at the meta or para positions of the aryl ring were explored using **2c**–**2j,** which were readily synthesized by reactions involving ethyl 3-aryl-3-oxypropanoates and ethyl 4-aminobenzoates, and cyclization of the resulting β-enamino esters **1** in hot diphenyl ether (Scheme 1B). Addition of an electron-donating group (**2c**, IC_{50} = 2.2 μM), -withdrawing groups (**2d**, IC_{50} = 2.1 μM and **2e**, IC_{50} = 4.5 μM), or a hydroxyl group (**2f**, IC_{50} = 475 nM) at the para position of the phenyl group resulted in substantial decreases in inhibitory activity against H1975 cells. Interestingly, while exploring the effects of meta substituents, we found that **2h** possessing a meta-fluorophenyl moiety had increased inhibitory activity (IC_{50} = 24 nM) against H1975 cells, whereas **2i** and **2j**, which bore a trifluoromethyl and a hydroxyl group respectively at the meta position of the phenyl ring showed substantially decreased potencies (IC_{50} = 780 nM and 1.95 μM, respectively) compared with that of AS1712. The introduction of a meta-methoxy group (**2g**) on the tail aryl ring slightly reduced activity (IC_{50} = 44 nM). The effects of substituents at the 6-position of the 4(1*H*)-quinolone scaffold were also explored by replacing the ethyl group with less or more sterically bulky groups (**2k**, IC_{50} = 207 nM and **2l**, IC_{50} = 48 nM, respectively) or by removal of the oxo group (**2m**, Scheme 1C, IC_{50} = 810 nM). The results showed that the original ethyl carbonate is the optimal substituent at the C-6 position. Overall, the data gained from the SAR study suggested that **2h** (denoted RJ-LC-15-8) possessed a greater anti-cellular proliferation potency (IC_{50} = 24 nM) against H1975 cells than did AS1712 and, therefore, deserves to be further developed into a drug for the treatment of cancers with MDR.

Table 2. Cell-based SAR study of AS1712 for the inhibition of H1975 cells

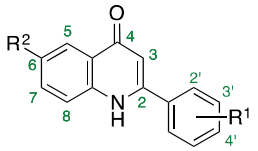

Compound	R^1	R^2	IC_{50}
AS1712	H	COOEt	33 ± 4.86 nM
2a	H	COOH	>5 μM
2b	H	CONHEt	3.7 ± 0.73μM
2c	4'-OMe	COOEt	2.2 ± 0.20μM
2d	4'-F	COOEt	2.1 ± 0.21 μM
2e	4'-Br	COOEt	4.5 ± 0.90μM
2f	4'-OH	COOEt	475 ± 31.6 nM
2g	3'-OMe	COOEt	44 ± 1.39 nM
2h(RJ-LC-15-8)	3'-F	COOEt	24 ± 1.12 nM
2i	3'-CF_3	COOEt	780 ± 12.1 nM
2j	3'-OH	COOEt	1.95 ± 0.20 μM
2k	H	COOMe	207 ± 39.1nM
2l	H	COO^iPr	48 ± 5.1 nM
2m	H	CH_2OEt	810 ± 0.12 nM

RJ-LC-15-8 Inhibited Tumor Growth Using a Mechanism Similar to AS1712 *In Vitro* and *In Vivo*

To verify that the mechanism of action of RJ-LC-15-8 is similar to AS1712, we performed additional experiments with H1975 cells. Immunoblotting showed that RJ-LC-15-8 induced cleavage of PARP and increased the expression of the mitotic phase markers cyclinB1 and p-HH3 (Figure S3A). *In situ* immunofluorescence of α-tubulin staining showed that RJ-LC-15-8 treatment inhibited microtubule polymerization (Figure S3B). The *in vitro* tubulin polymerization assay also showed direct inhibition by RJ-LC-15-8 of microtubule polymerization (Figure S3C). Next, we evaluated the anti-tumor ability of RJ-LC-15-8 using the H1975 xenograft model, and the data showed that, in

comparison with the control group, RJ-LC-15-8 inhibited tumor growth (average tumor size, 2153 ± 126.3 mm^3 for the DMSO control treatment and 1333 ± 121.9 mm^3 for the 4 mg/kg and 972.5 ± 52.3 mm^3 for the 8 mg/kg RJ-LC-15-8 treatments on day 21; both $p < 0.01$; Figure S3D). At the end of the experiment, we found that RJ-LC-15-8 treatment had not affected body mass (Figures S3E). We also evaluated the cytotoxicity of RJ-LC-15-8 against triple-negative breast cancer (TNBC). We found RJ-LC-15-8 was more effective than AS1712 in different TNBC cell lines, with IC_{50} values ranging from 21 to 35 nM (Figures S3F). The MDA-MB-231 xenograft model showed RJ-LC-15-8 could inhibit TNBC tumor growth in comparison with the control group (average tumor size, 218 ± 20.9 mm^3 for the DMSO control treatment and 105 ± 9.4 mm^3 for the 4 mg/kg and 73.6 ± 8.2 mm^3 for the 8 mg/kg RJ-LC-15-8 treatments on day 35; both $p < 0.05$; Figure S3G). RJ-LC-15-8 treatment did not affect body mass in MDA-MB-231 xenograft model (Figures S3H).

Scheme 2. Conjugate magnetic beads on AS1712.

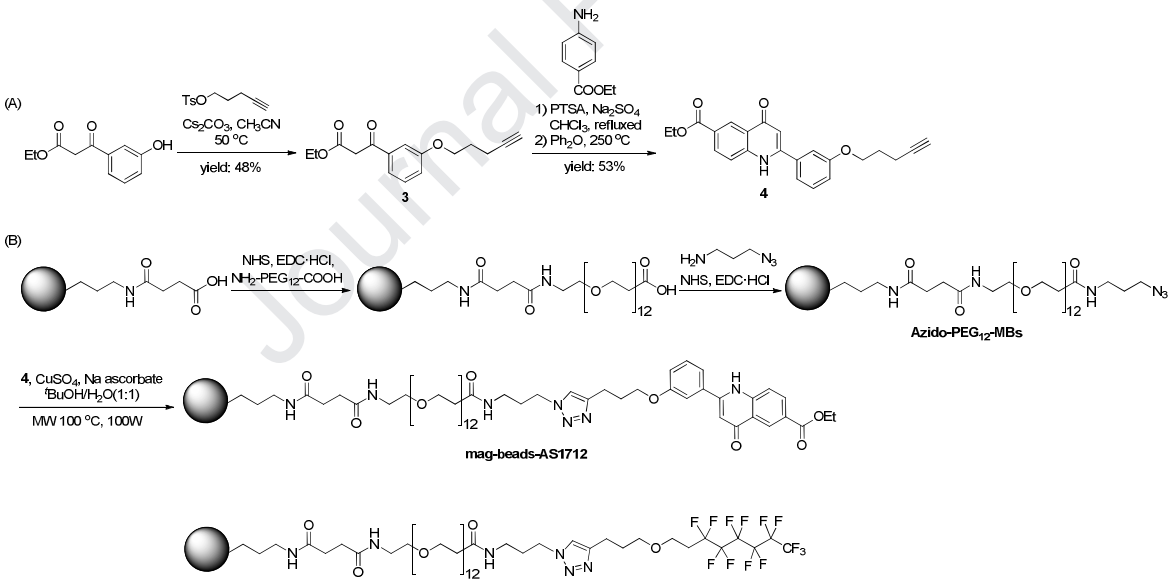

AS1712 Binds the Colchicine-Binding Pocket of β-Tubulin

Inhibition by AS1712 of microtubule polymerization led us to hypothesize that AS1712 directly targeted tubulin. To provide evidence for this hypothesis, we performed a pull-down assay using magnetic beads conjugated with AS1712. First, the alkyne **4** was synthesized via a three-step

procedure from ethyl 3-(3-hydroxyphenyl)-3-oxopropanoatealkyne (Scheme 2A) and then coupled to magnetic beads equipped with polyethylene glycol$_{12}$-azido linkers to generate "mag-beads-AS1712" (Scheme 2B). After incubating H1975 lysates separately with mag-beads-AS1712 or mag-beads-control overnight at 4 °C, immunoblotting showed that the mag-beads-AS1712 had pulled down only β-tubulin (Figure 4A). Next, we performed a surface plasmon resonance study to measure the value of the dissociation constant (K_D) for the tubulin-AS1712 complex. Different concentrations of AS1712 were injected over a tubulin-immobilized sensor chip surface, and the formation of complexes was monitored. The number of resonance units, which reflected the amount of complex formed, increased in a dose-dependent manner (Figure 4B). The K_D value for the complex was 13.8 μM as determined by fitting the data to a steady-state model. The data indicated that AS1712 directly interacted with tubulin.

We further characterized the AS1712-binding site on tubulin using a limited proteolysis assay. Two different tubulin-binding sites for microtubule-destabilizing agents are known: the vinca site and the colchicine site. When a drug binds to tubulin, it induces conformational changes that can be probed by a limited trypsin-digestion assay [28] (Figure 4C). The colchicine-site agent nocodazole caused β-tubulin to unfold and produced an increased amount of βcol after a limited trypsin digestion. In contrast, the vinca-site agent vincristine stabilized the α- and β-tubulin folds and decreased the amount of the βcol, αN, and αC fragments produced in comparison with the control digest. The tryptic pattern for the tubulin sample exposed to AS1712 was similar to that of nocodazole (Figure 4C). A competition assay was performed to confirm that AS1712 binds to the colchicine site. The binding site competition between the test compound and colchicine will decrease the intrinsic fluorescence of colchicine-tubulin complex by reducing the amount of colchicine bound [29]. The presence of AS1712 decreased the colchicine fluorescence in a dose-dependent manner as did nocodazole, whereas vincristine did not (Figure 4D).

We performed a molecular modeling study to explore the binding mode of AS1712 in the colchicine pocket of a heterodimeric tubulin crystal structure [30]. The orientation of colchicine, which was the original ligand in the crystal structure, was used as a reference. The binding pose of

AS1712 was generated by molecular docking into the colchicine binding pocket could be superimposed onto the colchicine structure with an RMSD value of 0.383 Å (Figure 4E). The docking energy score for the AS1712 complex (–32.8706 kcal/mol) was higher than that for the colchicine complex (–4.47969 kcal/mol). Various types of bonds were found between AS1712 and the α/β-tubulin dimer within a distance of 7 Å (Figure 4F), including hydrogen bonds between AS1712 and Ala250 and Lys254 of β-tubulin and Gln11 of α-tubulin, as well as pi-bonds with Leu248, Lys254, Met259, Ala316, and Lys352 of the β- tubulin (Figure 4G). These results suggested that AS1712 binds to β-tubulin at its colchicine-binding pocket.

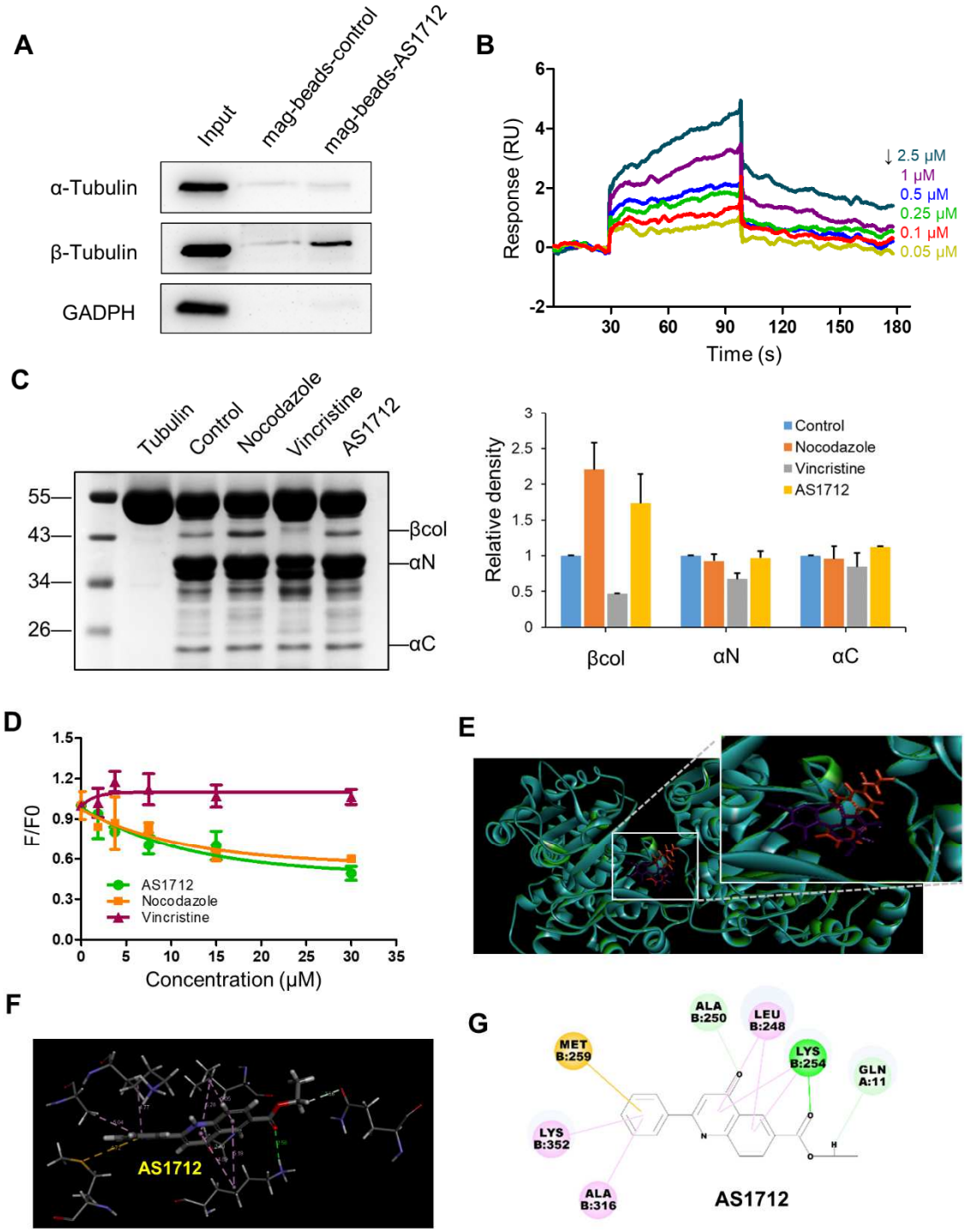

Figure 4. AS1712 binds to the colchicine-binding pocket of β-tubulin. (A) H1975 cell lysates were incubated with mag-beads-control or -AS1712 overnight and precipitated proteins were detected by immunoblotting. (B) Binding affinity of AS1712 to tubulin as measured by surface plasmon resonance. (C) Tubulin (1 mg/mL) was incubated with 100 μM of nocodazole, vincristine,

AS1712, or DMSO control for 30 min at 30 °C. Then, the samples were subjected to trypsin digestion for 10 min on ice. The positions of the tryptic cleavage products, αN, αC, and β-col, are shown to the right of the gel. Data are the mean ± SD. (D) Colchicine competition assay. AS1712 and nocodazole decreased the fluorescence of the colchicine-tubulin complex. Data are the mean ± SD. (E) Superimposition of the docked AS1712-tubulin (orange) and colchicine-tubulin complexes (purple). (F) Interactions between the tubulin heterodimer and AS1712. (G) Schematic of the AS1712 and tubulin-residue interactions.

AS1712 and RJ-LC-15-8 Overcame P-Glycoprotein–Mediated Multidrug Resistance

A major mechanism of MTA-induced MDR is P-gp overexpression, which is also the most common resistance mechanism that is clinically relevant to cancer therapy. Therefore, we tested the cytotoxic effects of AS1712 and RJ-LC-15-8 on the KBtax, KBvin, and CEM/VBL cancer cell lines, which overexpress P-gp. The KBtax and KBvin cell lines were developed by exposure of the human oral cancer cell line KB to paclitaxel and vincristine, respectively [31]. CEM/VBL cells were developed by exposure of the human T-lymphoblastic leukemia cell line CCRF-CEM to vinblastine [31]. The resistance factor (RF) values for the KBtax, KBvin, and CEM/VBL cells against paclitaxel were 10, 70, and 214, respectively, and the values against vincristine were 32, 163, and 440, respectively (Table 3). These results confirmed that these cell lines were resistant to paclitaxel and vincristine. By contrast, AS1712 and RJ-LC-15-8 were cytotoxic to these cell lines, and their effects on these cells were equal to or greater than those on the parent cells (Table 3). Notably, ixabepilone, a second-line MTA used for advanced breast cancer that no longer responds to available chemotherapies, did not effectively inhibit the viability of these multidrug resistant cell lines (Table 3).

Table 3. The cytotoxicity of AS1712 and RJ-LC-15-8 against KB, CCRF-CEM cells and their multidrug resistant sublines

Compound	KB	KBtax	RF[a]	KBvin	RF	CCRF-CEM	CEM/VBL	RF
	IC_{50} (nM)	IC_{50} (nM)		IC_{50} (nM)		IC_{50} (nM)	IC_{50} (nM)	
AS1712	37 ± 0.27	30 ± 0.65	0.81	37 ± 0.77	1	45 ± 0.45	44 ± 0.98	0.97
RJ-LC-15-8	34 ± 0.39	30 ± 1.35	0.88	35 ± 0.88	1	20 ± 1.71	16 ± 0.52	0.8
Paclitaxel	10 ± 0.32	101 ± 5.52	10	708 ± 46.9	70	4 ± 0.02	857 ± 9.89	214
Vincristine	5 ± 0.31	49 ± 2.96	32	817 ± 47.4	163	3 ± 0.04	1320 ± 20.6	440
Ixabepilone	8 ± 0.37	35 ± 0.71	4.3	193 ± 24.2	24	3 ± 0.06	150 ± 6.59	50

[a]RF, resistance factor (IC_{50} in resistant cell line/IC_{50} in parent cell line).

To assess the activity of RJ-LC-15-8 against tumor viability *in vivo*, BALB/c mice were grafted with KBtax cells and then intraperitoneally injected with DMSO, paclitaxel, (15 mg/kg), or RJ-LC-15-8 (8 mg/kg) three times a week (n = 5 per group). After 21 days of treatment, the RJ-LC-15-8 group showed substantially decreased tumor growth as compared with the paclitaxel and DMSO groups (average tumor size, 1109 ± 128.3 mm^3 for DMSO; 868.7 ± 121.4 mm^3 for paclitaxel; and 528.4 ± 101.6 mm^3 for RJ-LC-15-8; Figures 5A and S4A). TUNEL staining of the tumor tissues showed that the RJ-LC-15-8 treatment induced apoptosis (Figure 5B). Body mass and serum biochemical markers for liver and kidney functions were not negatively affected at the end of the experiment (Figures S4B and C). Thus RJ-LC-15-8 inhibited the growth of an MDR-type cancer tumor with low toxicity.

Because RJ-LC-15-8 displayed inhibitory activity against the KBtax cells, we sought to determine whether its effects were related to P-gp, either through a direct inhibition or because it is not a P-gp substrate. Therefore, we examined the effects of RJ-LC-15-8 on P-gp efflux activity and its expression. A rhodamine efflux assay showed that RJ-LC-15-8 did not directly inhibit pump activity in KBtax cells but that verapamil, a known P-gp inhibitor, did (Figure 5C). Our immunoblotting study showed that RJ-LC-15-8 did not affect P-gp expression in KBtax cells, whereas it induced cleavage of the apoptosis markers PARP and caspase-9 and increased the expression of the mitotic phase markers cyclin B1 and p-HH3 (Figure 5D). *In situ* immunofluorescence staining of α-tubulin showed that RJ-

LC-15-8 treatment inhibited microtubule polymerization and disrupted mitotic spindle organization (Figure 5E). RJ-LC-15-8 induced apoptosis in multidrug resistant cells without interfering directly with P-gp expression OR activity and, more broadly, the mechanism of cytotoxicity of RJ-LC-15-8 was not related to P-gp.

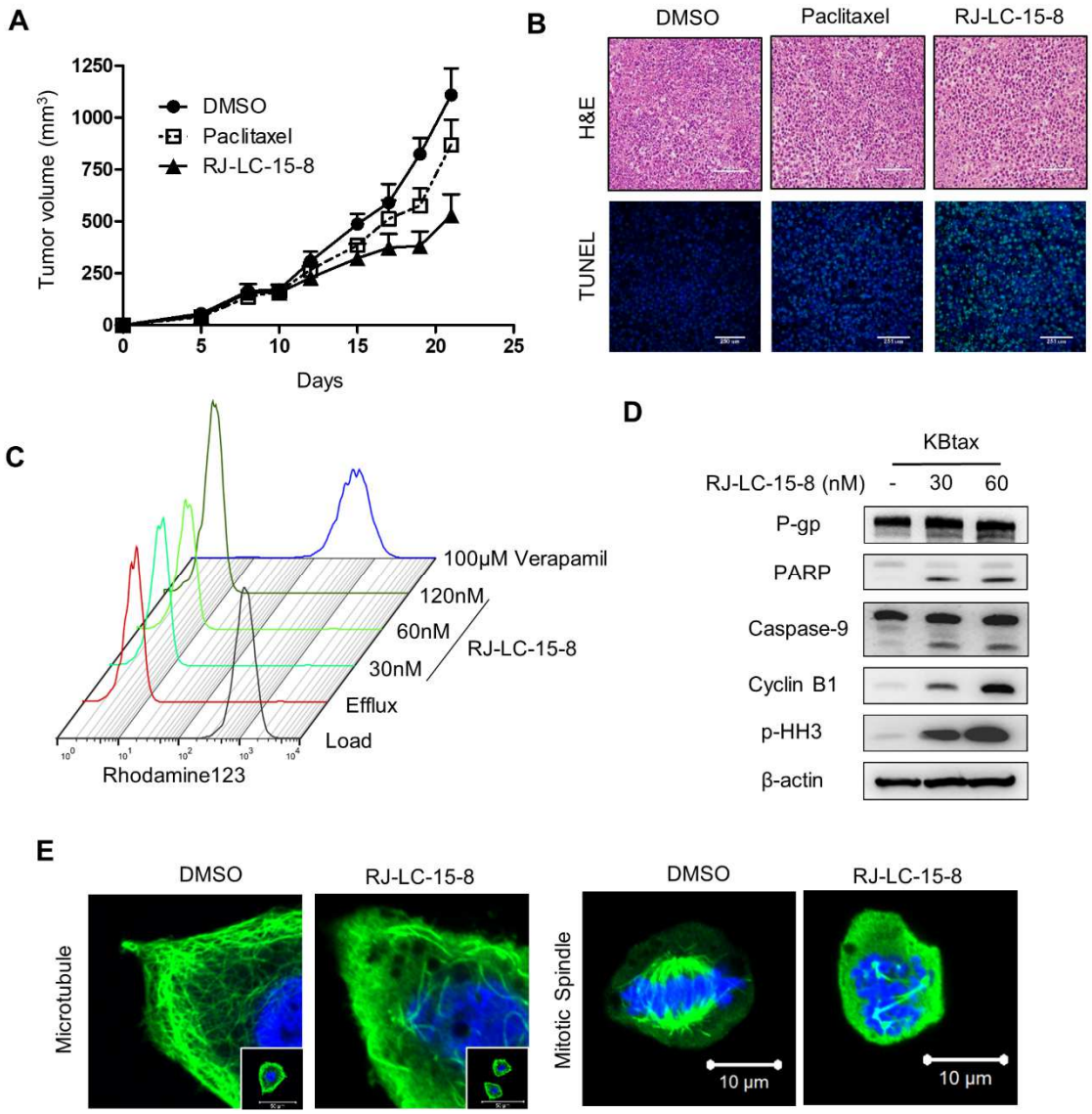

Figure 5. RJ-LC-15-8 inhibited KBtax tumor growth and induced apoptosis without interfering with P-gp. (A) KBtax (1×10^7) cells were subcutaneously injected into BALB/c nude mice. Mice were treated with DMSO, paclitaxel (15 mg/kg), or RJ-LC-15-8 (8 mg/kg) intraperitoneally three times a week for 21 days. The tumor volume was measured before each treatment. Data are shown as the

mean ± SEM. (B) Tumor slices were histologically stained with hematoxylin and eosin (H&E), and the cell apoptosis status was determined by TUNEL staining. (C) Rhodamine efflux assay for P-gp pumping activity. (D) Samples of KBtax cells were treated with one of the indicated concentrations of RJ-LC-15-8 for 24 h and then harvested to assess expression of the indicated proteins. (E) The microtubule networks and mitotic spindle organization in KBtax cells after a 6-h treatment with 30 nM RJ-LC-15-8.

Discussion

Cancer is the second leading cause of death worldwide and afflicts ~40% of the global population. Lung, breast, colorectal, and prostate cancers are the most common types and account for ~46% of all cancer deaths, with lung cancer being responsible for the highest number of deaths [1]. MTAs are widely used to treat advanced cancers, but prolonged treatment with MTAs reduces their clinical efficacy owing to the development of drug resistance by the cancers [32-34]. Thus, the development of new agents that improve drug efficacy and overcome drug resistance is an ongoing effort. For the study reported herein, we showed that AS1712 has the potential to treat various types of cancers and the ability to overcome MDR caused by MTAs with good efficacy and a good therapeutic window (Figure 6).

Cancer cells rely on microtubules to advance through mitosis and rapidly divide, which has made microtubules an important therapeutic target in cancer treatments for >50 years [35]. When MTAs alter microtubule dynamics, they cause mitotic arrest and trigger mitochondria-mediated intrinsic apoptosis [29, 36, 37]. We demonstrated that AS1712 inhibited microtubule polymerization and nucleation and disrupted mitotic spindle organization. AS1712 also induced mitotic arrest and then triggered release of cytochrome c and cleavage of caspase-9 to activate intrinsic apoptosis in several cancer cell lines (Figure 6). AS1712 also had good *in vivo* activity against tumor growth with no noticeable toxicity. The anti-cancer activities of AS1712 are similar to those of MTAs currently used clinically, although AS1712 has a different tubulin-binding site.

There are at least four binding sites on tubulin with a stabilizing or destabilizing function [38]. The colchicine-binding site is located on β-tubulin at its interface with α-tubulin [39]. Colchicine-binding site inhibitors (CBSIs) destabilize microtubule assembly and exhibit anti-angiogenesis and vascular-disruption activities, which are not found for inhibitors of the other functional sites [40, 41]. Unlike taxanes and vinca alkaloids, CBSIs can counteract the effects of overexpression of β-tubulin isoforms, and MDR mechanisms have little effect on CBSI activity [35, 42, 43]. Our results showed that AS1712 directly interacts with the colchicine-binding pocket of β-tubulin, indicating that AS1712 should be classified as a CBSI and suggested that, because of its binding site, AS1712 may not be susceptible to resistance induced by conformational changes in β-tubulin caused by mutations.

Currently, no CBSIs are approved for cancer therapy because colchicine and its derivatives are toxic to humans [38, 44]. However, AS1712 showed a >100-fold therapeutic window for the cell lines analyzed here and did not inhibit microtubule polymerization, cell-cycle arrest, or apoptosis in HFB cells at the highest treatment dosage that was used for the cancer cells. AS1712 also showed no notable toxicity in the animal model. Thus AS1712 may be a CBSI with low toxicity and has the potential to act as a lead compound for further development of anti-cancer agents.

MDR is a major cause of treatment failure in various cancer therapies [27]. Overexpression of P-gp is the main MDR mechanism involved in MTA-induced resistance because most MTAs, including paclitaxel, vincristine, vinblastine, and docetaxel, are exported from cells by P-gp [17, 45, 46]. P-gp pumps many different types of cytotoxic drugs out of cancer cells, thereby decreasing intracellular drug concentrations and resulting in treatment failure [46]. AS1712 inhibited the proliferation of KBtax, KBvin, and CEM/VBL cells that overexpressed P-gp with IC_{50} values comparable to those of their respective parental control cell lines. Our results suggested that AS1712 either directly inhibited P-gp activity or did not function as a P-gp substrate, thereby against P-gp–overexpressing cancer cells. Our rhodamine efflux assay and immunoblotting study ruled out the possibility that AS1712 directly inhibits P-gp pump activity or P-gp expression, which supports the hypothesis that AS1712 is not a P-gp substrate. Although other P-gp inhibitors, such as verapamil, cyclosporine, and valspodar, can reverse the MDR phenotype of cancer cells, clinical trials involving these inhibitors showed toxic side

effects and failed to improve clinical outcomes [47, 48]. With its inability to act as a P-gp substrate, AS1712 provides a different treatment strategy for MDR cancers. Ixabepilone is a second-line MTA used for treatment of advanced breast cancers that no longer respond to currently available chemotherapies [49, 50]; however, we found that some MDR cell lines resist treatment by ixabepilone, which thereby restricts its clinical use. In contrast, AS1712 has the potential to treat various types of cancers, including those of the lung, breast, ovary, prostate, and head and neck and leukemia that were first clinically subjected to taxanes or vinca alkaloids [14, 15]. Our results suggest that AS1712 or its derivative RJ-LC-15-8 may counteract multidrug resistance in various types of cancers.

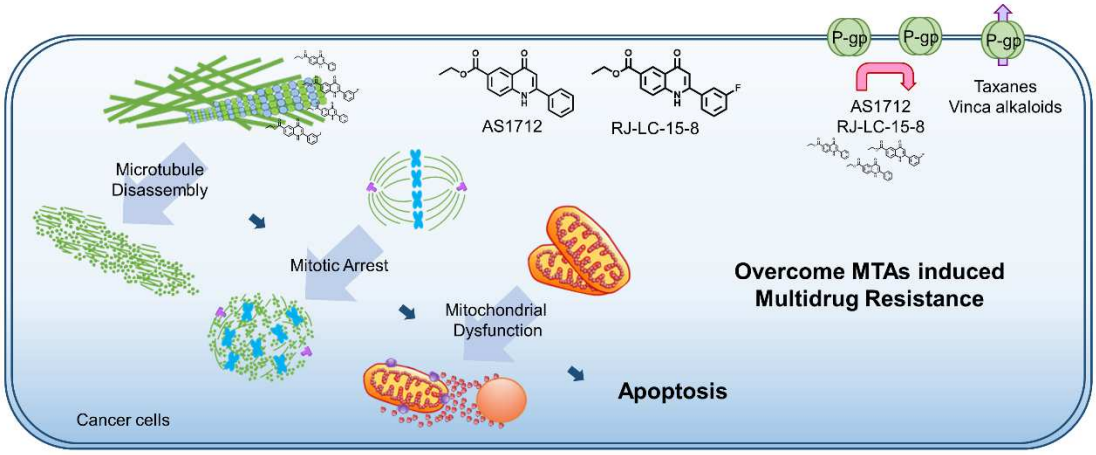

Figure 6. Proposed Mechanism of Action of AS1712 on anti-cancer effects.

Conclusions

For the study reported herein, we showed that AS1712 directly targets the colchicine-binding site of β-tubulin to disassemble microtubules, which subsequently induces mitotic arrest and activates apoptosis. AS1712 can overcome the MTAs-induced acquired resistance, including β-tubulin alterations and P-gp mediated multidrug resistance. We suggest that AS1712 and its derivative RJ-LC-15-8 may have great potential for cancer therapy.

Experimental section

Chemical library. We used the chemical library "GRC-2M" from Genomics Research Center at Academia Sinica. The 2-million compound library contains pure natural products, approved drugs, known bioactive inhibitors, commercial synthetic molecules, and proprietary collections. Compounds were prepared at 1 mM in 1536-well propylene plates.

Antibodies and Reagents. Antibodies against PARP, caspase-3, caspase-8, caspase-9, Bax, and MDR-1 were purchased from Cell Signaling. Antibodies against cyclin B1, cyclin A, GADPH, and MOCT-1 were obtained from Santa Cruz. Antibodies against α-tubulin, β-tubulin, and β-actin were from Sigma Aldrich. The antibody preparation against cytochrome c was from Abcam. The antibody preparation against p-HH3 (S10) was from Merck Millipore. Horseradish peroxidase–labeled anti-mouse and anti-rabbit antibodies were purchased from Santa Cruz. Fluorescein isothiocyanate–labeled anti-mouse antibody was from Thermo Fisher Scientific. Roswell Park Memorial Institute (RPMI) 1640 medium, Dulbecco's Modified Eagle medium (DMEM), and fetal bovine serum were purchased from GIBCO Life Technologies. The *in situ* cell death detection (TUNEL) kit was purchased from Roche. The tubulin polymerization assay kit was obtained from Cytoskeleton. The BCA protein assay kit was purchased from Pierce. The Series S Sensor Chip SA and HBS-EP+ running buffer were obtained from GE Healthcare.

Cell Lines and Cell Culture. We had isolated CL1-0 cells from a 64-year-old male patient with a poorly differentiated adenocarcinoma [51]. PC9 cells were obtained from Dr. C.H. Yang (Graduate Institute of Oncology, Cancer Research Center, National Taiwan University). Molt4 leukemia cells were obtained from Dr. Tang K. Tang (Institute of Biomedical Sciences, Academia Sinica). KB, KBtax, KBvin, CCRF-CEM, and CEM/VBL cells were obtained from Dr. T.C. Lee (Institute of Biomedical Sciences, Academia Sinica). The KB cell line was originally derived from an oral epidermal carcinoma and has been shown to be contaminated with HeLa cells [31]. Hs578T, MDA-

MB-231, 37T, and 82T cells were obtained from Dr. Y.S. Lu (Department of Internal Medicine, College of Medicine, National Taiwan University). 37T and 82T cells were isolated from breast cancer patients and cultured in 2% IH medium. SKOV-3, IGR-OV1, Ovcar-3, HCT116, HT-29, Colon205, SW620, Du-145, and PC-3 cells were obtained from Dr. S.L. Yu (Department of Clinical Laboratory Sciences and Medical Biotechnology, National Taiwan University). The NBE cell line was provided by Dr. Reen Wu (Department of Anatomy, Physiology and Cell Biology, University of California Davis) and cultured in bronchial epithelial basal medium. SAS and OECM1 cells were obtained from Dr. C.Y. Chen (Graduate Institute of Health Industry Technology and Research Center for Industry of Human Ecology, Chang Gung University of Science and Technology). A549, H1975, BT-549, and HFB cells were purchased from American Type Culture Collection (Rockville, MD, USA). In general, cells were cultured in RPMI 1640 medium or DMEM supplemented with 10% heat-inactivated fetal bovine serum and 1% penicillin-streptomycin in a humidified incubator under an atmosphere of 5% CO_2 and 95% air.

Cell Cytotoxicity Assay. Cells were seeded into the wells of 96-well plates (2000 cells/well). After an overnight culture, the cells were treated with different concentrations of a compound for 72 h. The CellTiter 96 AQueous one-solution cell proliferation assay (MTS) reagent was used to determine cytotoxicity. After treatment with a compound, 20 μL of the MTS reagent was added to each well and the plates were incubated at 37 °C for 1−4 h. Next, the absorbance at 490 nm of the culture medium in each well was determined using a VersaMax microplate reader (Molecular Devices).

Colony Formation Assay. Cells were seeded into the wells of six-well plates (1000 cells/well). After overnight culture, the cells were treated with various concentrations of AS1712 for 2 weeks. Then, the colonies in each well were fixed with 3.7% paraformaldehyde, stained with 0.04% crystal violet, and dissolved in 1 ml DMSO. The absorbance at 590 nm of each DMSO solution was read using the VersaMax microplate reader.

Cell Cycle Analysis. After treatment, cells were trypsinized and fixed in ice-cold 70% ethanol overnight. Fixed cells were washed with PBS and stained with 0.5 mL of a propidium iodide (10

μg/mL)/RNase (20 μg/mL) solution for 30 minutes. The cellular DNA content was analyzed with a FACSCanto flow cytometer (Becton Dickinson).

Immunoprecipitation and Immunoblotting. The cells were harvested and lysed in RIPA buffer (20 mM Tris-HCl, 150 mM NaCl, 1 mM Na_2EDTA, 1% sodium deoxycholate, 1% IGEPAL CA-630, 0.1% SDS, pH 7.5) with protease inhibitors (Roche). Protein concentration was measured by the BCA assay. For immunoprecipitation, protein extracts were incubated with mag-beads-AS1712 or mag-beads-control at 4 °C overnight and then washed five times with PBS before immunoblotting. For immunoblotting, equivalent amounts of denatured proteins were separated through SDS-PAGE gels and then transferred to PVDF membranes (Millipore), which were each blocked with 5% nonfat milk in PBS and 0.1% Tween-20 (Sigma Aldrich) for 1 h. Then each membrane was incubated with a primary antibody overnight at 4 °C, followed by incubation with a horseradish peroxidase–conjugated secondary antibody for 1 h at room temperature. The signal was visualized by enhanced chemiluminescence detection, and images were acquired using a BioSpectrum Imaging System (UVP).

Immunofluorescence Staining. Cells or microtubule asters were fixed with 3.7% paraformaldehyde, permeabilized with 0.1% Triton X-100, stained with anti-α-tubulin (1:1000 dilution) at 4 °C overnight, and then incubated with a fluorescein isothiocyanate–conjugated secondary antibody (1:500) at 37 °C for 1 h. Cells were then mounted with Prolong Gold Antifade Reagent and stained with DAPI (Thermo Fisher Scientific), after which images were acquired with an LSM 700 laser scanning confocal microscope (Carl Zeiss).

***In Vivo* Microtubule Assembly Assay.** Cell samples were treated with a compound for 6 h, and the cells were then harvested and were lysed in 20 mM Tris-HCl, 1 mM $MgCl_2$, 2 mM EGTA, 0.5% IGEPAL CA-630, 2 mM PMSF, 200 U/mL aprotinin, and a protease inhibitor cocktail (pH 6.8). After centrifugation of each lysate at 16,000 rpm for 15 min at room temperature, its supernatant containing soluble monomeric tubulin and the particulate fraction containing polymerized tubulin were separately subjected to immunoblotting.

***In Vitro* Tubulin Polymerization Assay.** Reagents from a Tubulin Polymerization Assay kit (Cytoskeleton) were used according to the manufacturer's instructions. Purified porcine tubulin (4 mg/mL; >99% purity) in G-PEM buffer (80 mM PIPES, 2 mM $MgCl_2$, 0.5 mM EGTA, 1 mM GTP, 15% glycerol, pH 6.9) was mixed with each test compound in the wells of a 96-well plate. Then, the A_{340} value was recorded each minute for 1 h at 37 °C with the VersaMax microplate reader.

***In Vitro* Microtubule Nucleation Assay.** Purified centrosomes were incubated with or without AS1712 and with porcine tubulin (Cytoskeleton) in 80 mM PIPES, 1 mM $MgCl_2$, 1 mM EGTA, and 1 mM GTP, pH 6.8 for 8 min at 37 °C. Microtubule asters were fixed in 1% glutaraldehyde, sedimented onto acid-treated coverslips, and finally subjected to immunofluorescence with anti-α-tubulin. The fiber lengths of the microtubule asters were measured using MetaMorph image analysis software (n = 20/group).

Binding Affinity Assay. Surface plasmon resonance technology was used to analyze the binding affinity of AS1712 for tubulin. A Series S Sensor Chip SA was conditioned with three consecutive 1-min injections of 1 M NaCl in 50 mM NaOH, and then 50 μg/mL biotin-tubulin (Cytoskeleton) was immobilized onto the sensor chip surface in a Biacore T200 system (GE Healthcare) to attain 3,000 resonance units. One flow cell on the chip was left free to serve as the negative control. Biocytin (Sigma Aldrich) was used to block any remaining unmodified streptavidin sites. Different concentrations of AS1712 in 10 mM HEPES, 150 mM NaCl, 3 mM EDTA, and 0.05% surfactant P20, pH 7.4 were separately injected over the sensor chip surface to measure the association and dissociation of AS1712 and tubulin at 25 °C. The value of K_D was calculated using the steady-state fitting mode in Biacore T200 Evaluation Software.

Limited Proteolysis Assay. Tubulin (1 mg/mL) was incubated individually with a test compound for 30 min at 30 °C in 0.1 M morpholino ethanesulfonic acid, 1 mM $MgCl_2$, 1 mM EGTA, pH 6.9, and then 25 μg/mL trypsin (TPCK-treated, Sigma Aldrich; 1:40 [w/w] trypsin/tubulin) was added to the solution for a 10-min digestion at 4 °C. Samples were electrophoresed through a 15% SDS-PAGE gel and stained with Coomassie brilliant blue R250. The images were scanned and quantified using a BioSpectrum Imaging System (UVP).

Colchicine Competition Assay. Tubulin (3 μM) was mixed with colchicine (3 μM) and then incubated with the various concentrations of AS1712, nocodazole, or vincristine in PEM buffer (80 mM PIPES, 2 mM $MgCl_2$, 0.5 mM EGTA, pH 6.9) at 37 °C for a total volume of 100 μl per well in black 96-well plates for 1 h. Fluorescence intensities (excitation and emission wavelengths at 365 and 435 nm, respectively) were recorded using an Infinite M200 plate reader (Tecan). Fluorescence values were normalized to the DMSO control.

Molecular Modeling. The DMA-colchicine-bound tubulin heterodimer crystal structure (PDB-ID: 1SA0) [30] was used for the docking study. Molecular docking was conducted using Discovery Studio (Accelrys Inc.) to assess the probably binding mode of AS1712 in the colchicine-binding site of tubulin. The initial crystal structure was prepared using the Prepare Protein protocol in Discovery Studio that protonates the structure and inserts missing loop regions. The docking was performed using the CDOCKER [52] docking protocol in Discovery Studio based on the grid-based molecular docking method and the CHARMm force field for binding-energy minimization. Random ligand conformations were generated from each initial ligand structure via random rotations and high-temperature molecular dynamics. The random conformations were refined by grid-based simulated annealing and minimization. The pose was each chosen based on their highest docking score for further interaction analyses. The post-docking analyses were performed using the View Interactions tool in Discovery Studio to identify the ligand-protein hydrogen bonds, bumps, and Pi interactions.

Rhodamine Efflux Assay. KBtax cells (2.5×10^5/test) were collected and held on ice for 1 h in cold medium with 5 mM rhodamine. Then, the cells were resuspended in medium warmed to 37 °C with one of the indicated compounds and incubated for 1 h in a water bath at the same temperature for efflux determination. The fluorescence intensities were quantified by FACSCanto flow cytometry.

Xenograft Tumor Model. Using the H1975, MDA-MB-231, and KBtax xenograft models, tumors were established after inoculation into the right flanks of 6-week-old BALB/c nude mice (NARLabs, Taipei, Taiwan). After establishment of the tumors, vehicle and test compounds, which had been dissolved in DMSO, were each injected intraperitoneally into a separate group of animals

three times per week. The body mass of each animal and tumor volumes were measured before each drug delivery. Tumor volume was calculated as $0.5W^2L$ (with W being the width of the smaller diameter and L being the length of the larger diameter). The animal experiment was carried out in accordance with the procedures and guidelines of the Institutional Animal Care and Use Committee, Institute of Biomedical Sciences, Academia Sinica.

Chemistry

General. Anhydrous solvents were freshly dried and purified by conventional methods prior to use. The progress of all the reactions were monitored by TLC, using TLC glass plates precoated with silica gel 60 F254 (Merck). Column chromatography was performed on silica gel Geduran® Si 60 (Merck). ^{1}H and ^{13}C NMR spectra were recorded with Bruker AV-III 400 MHz, Bruker N-600, Bruker AV-400, or AV-500 MHz spectrometers and chemical shifts were measured in δ (ppm) with residual solvent peaks as internal standards ($CDCl_3$, δ 7.26 ppm in ^{1}H NMR, δ 77 ppm in ^{13}C NMR; CD_3OD, δ 3.31 ppm in ^{1}H NMR, δ 49.0 ppm in ^{13}C NMR; DMSO-d_6, δ 2.50 ppm in ^{1}H NMR, δ 39.52 ppm in ^{13}C NMR). Coupling constants (*J*) are reported in hertz, and the splitting abbreviations used were as follows: s, singlet; d, doublet; t, triplet; m, multiplet. Melting points were recorded on Buchi 565 apparatus.

General Procedure for Synthesis of AS1712 and analogues. A solution of 4-substituted aniline (0.616 mmol), benzoylacetate (0.71 mmol), $TsOH\cdot H_2O$ (0.03 mmol) and Na_2SO_4 (6.16 mmol) in $CHCl_3$ (3 ml) was stirred and refluxed for 48h. The reaction mixture was concentrated in vacuo and washed with hexane or Et_2O. Next, collected filtrate and evaporated to get imine. The imine was dissolved in diphenylether (1 ml) and heated to 250°C for 10 mins. The reaction mixture was cooled to room temperature. After trituration with Et_2O, the product was collected by filtration.

Ethyl 4-oxo-2-phenyl-1,4-dihydroquinoline-6-carboxylate (AS1712). The title compound was prepared by following general procedure. Yield: 79%; Mp 308-311°C; ^{1}H NMR (600 MHz, DMSO-d_6) δ 11.98 (s, 1H), 8.71 (s, 1H), 8.17 (dd, *J* = 8.7 Hz, *J* = 1.5 Hz, 1H), 7.87-7.83 (m, 3H), 7.61-7.58 (m, 3H), 6.43 (s, 1H), 4.35 (q, *J* = 7.1 Hz, 2H), 1.36 (t, *J* = 7.2 Hz, 3H); ^{13}C NMR (150 MHz, DMSO-d_6)

δ 177.1, 165.8, 151.4, 144.1, 134.4, 132.0, 131.2, 129.5, 128.0, 127.5, 124.8, 124.6, 120.0, 108.7, 61.3, 14.7.

Ethyl 2-(4-methoxyphenyl)-4-oxo-1,4-dihydroquinoline-6-carboxylate (2c). The title compound was prepared by following general procedure. Yield: 73%; Mp 325-330°C; IR (neat): 3260, 3159, 2981,1697, 1635, 1574, 1538, 1486, 1456, 1395, 1248, 1230, 1191, 1124, 1022, 820, 786 cm-1; ^{1}H NMR (600 MHz, DMSO-d_6) δ 11.84 (s, 1H), 8.69 (s, 1H), 8.15 (dd, *J* = 8.7 Hz, *J* = 2.2 Hz, 1H), 7.95-7.90 (m, 2H) , 7.83 (d, *J* = 8.5 Hz, 1H), 7.14 (d, *J* = 8.5 Hz, 1H), 6.40 (s, 1H), 4.35 (q, *J* = 7.2 Hz, 2H) , 3.85 (s, 3H), 1.36 (t, *J* = 7.1 Hz, 3H); ^{13}C NMR (150 MHz, DMSO-d_6) δ 177.2, 165.8, 161.8, 150.9, 143.9, 132.0, 129.5, 127.5, 126.3, 124.7, 124.5, 119.7, 114.9, 108.0, 61.3, 56.0, 14.7. HRMS (ESI) *(m/z)*: calculated for $C_{19}H_{16}NO_4$ [(M-H)$^-$] 322.1079, found 322.1084.

Ethyl 2-(4-fluorophenyl)-4-oxo-1,4-dihydroquinoline-6-carboxylate (2d). The title compound was prepared by following general procedure. Yield: 83%; Mp 335-340°C; IR (neat): 3261, 3145, 3083, 2979, 2912, 1711, 1639, 1552, 1502, 1487, 1417, 1391, 1257, 1223, 1130, 1111, 1027, 923, 844, 774, 761 cm-1; ^{1}H NMR (600 MHz, DMSO-d_6) δ 11.97 (s, 1H), 8.70 (s, 1H), 8.18 (dd, *J* = 8.5 Hz, *J* = 1.9 Hz, 1H), 7.95-7.90 (m, 2H) , 7.83 (d, *J* = 9.0 Hz, 1H), 7.44 (t, *J* = 8.5 Hz, 1H), 6.42 (s, 1H), 4.35 (q, *J* = 7.1 Hz, 2H), 1.36 (t, *J* = 7.2 Hz, 3H); ^{13}C NMR (150 MHz, DMSO-d_6) δ 177.2, 165.8, 164.8, 163.2, 150.2, 143.9, 132.1, 130.7, 130.5, 130.5, 127.5, 124.9, 124.5, 119.8, 116.6, 116.4, 108.9, 61.3, 14.7. HRMS (ESI) *(m/z)*: calculated for $C_{18}H_{13}NO_3F$ [(M-H)$^-$] 310.0879, found 310.0871.

Ethyl 2-(4-bromophenyl)-4-oxo-1,4-dihydroquinoline-6-carboxylate (2e). The title compound was prepared by following general procedure. Yield: 87%; Mp 345-350°C; IR (neat): 3255, 3140, 3085, 2976, 1711, 1638, 1571, 1491, 1409, 1364, 1269, 1254, 1074, 1010, 914, 820, 776, 764 cm-1; ^{1}H NMR (600 MHz, DMSO-d_6) δ 11.99 (s, 1H), 8.70 (s, 1H), 8.18 (dd, *J* = 8.6 Hz, *J* = 1.9 Hz, 1H), 7.85-7.79 (m, 5H), 6.45 (s, 1H), 4.35 (q, *J* = 6.9 Hz, 2H), 1.37 (t, *J* = 7.2 Hz, 3H); ^{13}C NMR (150 MHz, DMSO-d_6) δ 177.3, 165.7, 150.0, 143.9, 133.4, 132.5, 132.2, 130.1, 127.5, 124.9, 124.8, 124.6, 119.8, 109.0, 61.3, 14.7. HRMS (ESI) *(m/z)*: calculated for $C_{18}H_{13}NO_3Br$ [(M-H)$^-$] 370.0079, found 370.0081.

Ethyl 2-(4-hydroxyphenyl)-4-oxo-1,4-dihydroquinoline-6-carboxylate (2f). The title compound was prepared by following general procedure. Yield: 48%; Mp 313-316°C; IR (neat): 3252, 3148, 3082, 2986, 2906, 1715, 1638, 1557, 1505, 1496, 1487, 1443, 1262, 1231, 1174, 1128, 1028, 965, 898, 839, 804, 789, 772, 755, 705, 667 cm-1; ^{1}H NMR (600 MHz, DMSO-d_6) δ 11.76 (s, 1H), 10.11 (s, 1H), 8.69 (s, 1H), 8.14 (dd, *J* = 9.0 Hz, *J* = 1.8 Hz, 1H), 7.83 (d, *J* = 8.6 Hz, 1H), 7.71 (d, *J* = 8.7 Hz, 2H), 6.95 (d, *J* = 8.9 Hz, 2H), 6.34 (s, 1H), 4.35 (q, *J* = 7.0 Hz, 2H), 1.36 (t, *J* = 7.1 Hz, 3H); ^{13}C NMR (150 MHz, DMSO-d_6) δ 176.6, 165.3, 159.9, 150.7, 143.4, 131.4, 129.0, 127.0, 124.1, 124.0, 119.1, 115.8, 107.0, 60.8, 14.2. HRMS (ESI) *(m/z)*: calculated for $C_{18}H_{14}NO_4$ [(M-H)$^-$] 308.0923, found 308.0930.

Ethyl 2-(3-methoxyphenyl)-4-oxo-1,4-dihydroquinoline-6-carboxylate (2g). The title compound was prepared by following general procedure. Yield: 85%; Mp 277-280°C; IR (neat): 3140, 3077, 2968, 1713, 1643, 1550, 1504, 1265, 1235, 1128, 1032, 882, 840, 771, 754, 706, 669 cm-1; ^{1}H NMR (600 MHz, DMSO-d_6) δ 11.93 (s, 1H), 8.71 (s, 1H), 8.18 (dd, *J* = 9.0 Hz, *J* = 1.5 Hz, 1H), 7.85 (d, *J* = 8.5 Hz, 1H), 7.51 (t, *J* = 8.2 Hz, 1H), 7.43-7.38 (m, 2H), 7.17 (d, *J* = 8.5 Hz, 1H), 6.45 (s, 1H), 4.36 (q, *J* = 7.1 Hz, 2H), 3.87 (s, 3H), 1.36 (t, *J* = 7.2 Hz, 3H); ^{13}C NMR (150 MHz, DMSO-d_6) δ 177.3, 165.8, 160.0, 151.0, 143.8, 135.6, 132.1, 130.7, 127.5, 124.8, 124.6, 120.2, 119.8, 116.9, 113.4, 108.9, 61.3, 55.9, 14.7. HRMS (ESI) *(m/z)*: calculated for $C_{19}H_{16}NO_4$ [(M-H)$^-$] 322.1079, found 322.1085.

Ethyl 2-(3-fluorophenyl)-4-oxo-1,4-dihydroquinoline-6-carboxylate (2h). The title compound was prepared by following general procedure. Yield: 88%; Mp 307-310°C; IR (neat): 3247, 3143, 3079, 2981, 2901, 1715, 1639, 1583, 1505, 1486, 1444, 1264, 1233, 1174, 1130, 1026, 901, 840, 790, 773, 756, 706 cm-1; ^{1}H NMR (600 MHz, DMSO-d_6) δ 11.98 (s, 1H), 8.71 (s, 1H), 8.19 (dd, *J* = 9.1 Hz, *J* = 2.4 Hz, 1H), 7.85 (d, *J* = 8.7 Hz, 1H), 7.79-7.70 (m, 2H), 7.68-7.63 (m, 1H), 7.45 (t, *J* = 8.7 Hz, 1H), 6.48 (s, 1H), 4.37 (q, *J* = 7.1 Hz, 2H), 1.37 (t, *J* = 7.2 Hz, 3H); ^{13}C NMR (150 MHz, DMSO-d_6) δ 177.3, 165.7, 163.5, 161.9, 149.7, 143.8, 136.5, 132.2, 131.7, 131.6, 127.5, 125.0, 124.6, 124.2, 119.9, 118.0, 117.9, 115.1, 114.9, 109.2, 61.3, 14.7. HRMS (ESI) *(m/z)*: calculated for $C_{18}H_{13}NO_3F$ [(M-H)$^-$] 310.0879, found 322.0873.

Ethyl 4-oxo-2-(3-(trifluoromethyl)phenyl)-1,4-dihydroquinoline-6-carboxylate (2i). The title compound was prepared by following general procedure. Yield: 82%; Mp 320-325°C; IR (neat): 3255, 3140, 3082, 2984, 2906, 1715, 1637, 1582, 1505, 1486, 1443, 1262, 1174, 1128, 1111, 1025, 840, 804, 789, 772, 755, 705, 668 cm-1; ^{1}H NMR (600 MHz, DMSO-d_6) δ 12.08 (s, 1H), 8.72 (s, 1H), 8.24-8.15 (m, 3H), 7.97 (d, *J* = 8.0 Hz, 1H), 7.84 (t, *J* = 8.2 Hz, 2H), 6.52 (s, 1H), 4.37 (q, *J* = 7.1 Hz, 2H), 1.37=8 (t, *J* = 7.1 Hz, 3H); ^{13}C NMR (150 MHz, DMSO-d_6) δ 177.3, 165.7, 149.6, 143.9, 135.3, 132.3, 130.7, 130.5, 130.3, 130.1, 129.9, 127.7, 127.5, 125.3, 125.0, 124.7, 123.5, 119.9, 109.6, 61.3, 14.7. HRMS (ESI) *(m/z)*: calculated for $C_{19}H_{13}NO_3F_3$ [(M-H)$^-$] 360.0848, found 360.0842.

Ethyl 2-(3-hydroxyphenyl)-4-oxo-1,4-dihydroquinoline-6-carboxylate (2j). The title compound was prepared by following general procedure. Yield: 27%; Mp 268-309 ^{o}C; IR (neat): 3204, 1724, 1583, 1500, 1488, 1272, 1135, 833, 759, 711, 683 cm-1; ^{1}H NMR (600 MHz, DMSO-d_6) δ 11.92 (s, 1H), 9.88 (s, 1H), 8.70 (s, 1H), 8.17 (dd, *J*=1.4, 8.7 Hz,1H), 7.84 (d, *J*=8.7 Hz,1H), 7.39 (t, *J*=7.9 Hz,1H),7.24 (d, *J*=7.5 Hz,1H), 7.18 (s, 1H), 6.99 (d, *J*=7.6 Hz,1H), 6.33(s, 1H), 4.36 (q, *J*=7.1 Hz,2H), 1.36 (t, *J*= 7.1 Hz, 3H); ^{13}C NMR (125 MHz, DMSO-d_6) δ 177.3, 165.8, 158.2, 151.3, 143.8, 135.6, 132.0, 130.7, 127.5, 124.8, 124.6, 119.8, 118.6, 118.1, 114.6, 108.6, 61.3, 14.7; HRMS (ESI) *(m/z)*: calculated for $C_{18}H_{15}NO_4$ [M+H]$^+$ 310.1079, found 310.1079.

Methyl 4-oxo-2-phenyl-1,4-dihydroquinoline-6-carboxylate (2k). The title compound was prepared by following general procedure. Yield: 82%; Mp 357-360°C; IR (neat): 3252, 3143, 3082, 2978, 1704, 1636, 1578, 1489, 1437, 1395, 1279, 1257, 1236, 1119, 973, 840, 768, 697, 683, 669 cm-1; ^{1}H NMR (600 MHz, DMSO-d_6) δ 11.98 (s, 1H), 8.73 (s, 1H), 8.18 (d, *J* = 8.9 Hz, 1H), 7.89-7.83 (m, 3H), 7.64-7.59 (m, 3H), 6.42 (s, 1H), 3.91 (s, 3H); ^{13}C NMR (150 MHz, DMSO-d_6) δ 177.3, 166.3, 151.3, 143.9, 134.3, 132.0, 131.2, 129.5, 128.0, 127.7, 124.7, 124.6, 119.9, 108.9, 52.7. HRMS (EI) *(m/z)*: calculated for $C_{17}H_{13}NO_3$ [(M)$^+$] 279.0895, found 279.0900.

Isopropyl 4-oxo-2-phenyl-1,4-dihydroquinoline-6-carboxylate (2l). The title compound was prepared by following general procedure. Yield: 73%; Mp 291-294°C; IR (neat): 3260, 3146, 3085, 2973, 1713, 1644, 1580, 1549, 1497, 1266, 1128, 838, 750, 690, 683 cm-1; ^{1}H NMR (600 MHz, DMSO-d_6) δ 11.97 (s, 1H), 8.70 (s, 1H), 8.18 (dd, *J* = 8.5 Hz, *J* = 1.8 Hz, 1H), 7.88-7.84 (m, 3H),

7.63-7.59 (m, 3H), 6.43 (s, 1H), 5.19 (sept, J = 6.2 Hz, 1H), 1.37 (d, J = 6.2 Hz, 6H); ^{13}C NMR (150 MHz, DMSO-d_6) δ 177.3, 165.3, 151.2, 143.9, 134.3, 132.1, 131.2, 129.5, 128.0, 127.5, 125.2, 124.6, 119.8, 108.8, 68.7, 22.2. HRMS (EI) *(m/z)*: calculated for $C_{19}H_{17}NO_3$ [$(M)^+$] 307.1208, found 307.1206.

4-oxo-2-phenyl-1,4-dihydroquinoline-6-carboxylic acid (2a). To a test tube equipped with a stir bar and septum was added AS1712 (50 mg, 0.17 mmol), 1:9 EtOH/H_2O (1.9 ml) and NaOH (70 mg, 1.71 mmol). The resulting mixture was stirred at 40°C for 4 h. After removal of EtOH in vacuo, the mixture was acidified with 10% HCl and collected the white precipitate. Yield: 99%. Mp 285-290°C; ^{1}H NMR (400 MHz, DMSO-d_6) δ 12.06 (s, 1H), 8.70 (s, 1H), 8.16 (d, J = 8.7 Hz, 1H), 7.91 -7.84 (m, 3H) , 7.62-7.58 (m, 3H), 6.40 (s, 1H); ^{13}C NMR (100 MHz, DMSO-d_6) δ 177.4, 167.3, 151.1, 143.7, 134.3, 132.3, 131.1, 129.5, 128.0, 127.7, 125.8, 124.6, 119.6, 108.7.

N-ethyl-4-oxo-2-phenyl-1,4-dihydroquinoline-6-carboxamide (2b). To a dry and N_2-flushed 10mL Schlenk flask equipped with stir bar and septum was added 2a (10 mg, 0.038 mmol) and CDI (6.4 mg, 0.04 mmol) in anhydrous DMF (0.8 ml). The reaction mixture was stirred at room temperature for 4 h, then treated with TEA (7.9 μL, 0.057 mmol), ethylamine hydrochloride (4.6 mg, 0.057 mmol) and stirred for overnight. After completion of the reaction, the DMF was removed in vacuo and purified by column chromatography to give solid product. Yield: 64%. Mp 330-340°C; IR (neat): 3561, 3271, 3070, 2969, 1629, 1577, 1494, 1295, 1253, 1149, 1081, 1048, 969, 914, 836, 803, 765, 692, 681 cm-1; ^{1}H NMR (600 MHz, $CD_3OD/CDCl_3$) δ 8.59 (s, 1H), 8.15 (d, J = 8.8 Hz 1H), 7.76-7.71 (m, 3H) , 7.56-7.52 (m, 3H), 6.59 (s, 1H), 3.46 (q, J = 7.4 Hz, 2H), 1.26 (t, J = 7.4 Hz, 3H) ; ^{13}C NMR (150 MHz, $CD_3OD/CDCl_3$) δ 179.4, 167.5, 152.4, 142.3, 133.9, 131.6, 130.9, 130.1, 129.1, 127.3, 123.9, 123.5, 118.9, 108.6, 35.0, 14.3. HRMS (ESI) *(m/z)*: calculated for $C_{18}H_{17}N_2O_2$ $[M+H]^+$ 293.1290, found 293.1287.

6-(ethoxymethyl)-2-phenylquinolin-4(1H)-one (2m). To a flask equipped with a stir bar and septum was added AS1712 (100 mg, 0.341mmol) in anhydrous THF (0.7 ml), then dropwise DIBAL-H (0.85 ml, 1.2M in toluene) under ice bath and N_2 atmosphere. After stirred at 0°C for 1h, the solution was quenched with MeOH and evaporated to get crude. The crude was purified by flash

column chromatography (MeOH/DCM) to afford primary alcohol. Next, the primary alcohol (80 mg, 0.318 mmol) was suspended on anhydrous Et_2O (1.1 ml) and slowly treated with PBr_3 (30 μL, 0.318 mmol) on N_2 atmosphere. After refluxed 2h, the mixture was quenched with H_2O and collected solid product by filtration. Finally, the benzylbromide (100 mg, 0.318 mmol) was suspended on EtOH (10.6 ml) and treated with DIPEA (498 μL, 2.86 mmol). After stirred at room temperature for overnight, the clear solution was evaporated the solvent and purified by flash column chromatography (MeOH/DCM) to afford product. Yield: 46%; Mp 218-222°C; IR (neat): 3059, 2966, 2925, 2853, 1649, 1594, 1577, 1543, 1500, 1252, 1097, 1084, 800, 773, 696, 684, 664, 560, 516 cm-1; ^{1}H NMR (600 MHz, $CDCl_3$) δ 10.08 (s, 1H), 8.24 (s, 1H), 7.69-7.64 (m, 4H), 7.46-7.43 (m, 3H), 6.43 (s, 1H), 4.57 (s, 2H), 3.54 (q, *J* = 7.2 Hz, 2H), 1.23 (t, *J* = 7.1 Hz, 3H); ^{13}C NMR (150 MHz, $CDCl_3$) δ 178.9, 150.8, 140.1, 134.4, 132.0, 130.4, 129.0, 127.2, 124.9, 124.4, 118.9, 108.2, 72.3, 65.8, 15.2. HRMS (EI) *(m/z)*: calculated for $C_{18}H_{17}NO_2$ [$(M)^+$] 279.1259, found [$(M)^+$] 279.1253.

Ethyl 3-oxo-3-(3-(pent-4-yn-1-yloxy)phenyl)propanoate (3). The mixture of ethyl 3-(3-hydroxyphenyl)-3-oxopropanoate (30 mg, 0.144 mmol) and Cs_2CO_3 (47 mg, 0.144 mmol) in acetonitrile (1 mL) was added a solution of pent-4-yn-1-yl 4-methylbenzenesulfonate (35 mg, 0.144 mmol) in acetonitrile at room temperature and heated to 50 ^{o}C for 26h. The reaction mixture was cooled down, filtered through cotton, evaporated solvent, and extracted with EA. Combined organic layers were dried over Na_2SO_4, then filtered and concentrated under vacuo to obtain the crude, which then purified by column chromatography (CH_2Cl_2/*n*-Hexane) to afford ethyl 3-oxo-3-(3-(pent-4-yn-1-yloxy)phenyl)propanoate as a colorless liquid with keto-enol tautomers. Yield: 48%. ^{1}H NMR (600 MHz, $CDCl_3$) δ 12.56 (s, 0.2H, enol form), 7.49 (m, 2H), 7.37 (t, *J*=7.9 Hz, 1H), 7.13 (dd, *J*=2.2, 8.2 Hz, 1H), 5.65 (s, 0.2H, enol form), 4.26(q, *J*=7.0 Hz, 0.4H, enol form), 4.21 (q, *J*=7.2 Hz, 2H), 4.12 (t, *J*=6.0 Hz, 2.4H, keto+enol), 3.97(s, 2H), 2.41 (td, *J*=2.4, 7.0 Hz, 2.4H, keto+enol), 2.02 (quin, *J*=6.5 Hz, 2.6H, keto+enol), 1.98 (t, *J*=2.5 Hz, 1H), 1.33 (t, *J*=7.1 Hz, 0.6H), 1.26 (t, *J*=7.1 Hz, 3H); ^{13}C NMR (150 MHz, $CDCl_3$) δ 192.3, 173.2 (enol form), 171.3 (enol form), 167.5, 159.3, 159.0 (enol form), 137.4, 134.9 (enol form), 129.8, 129.6 (enol form), 121.2, 120.7, 118.5 (enol form), 117.8 (enol form), 113.3, 111.9 (enol form), 87.6 (enol form), 83.4 (enol form), 83.2, 69.1, 69.0 (enol form),

66.4, 66.3 (enol form), 61.5, 60.3 (enol form), 46.1, 28.1 (enol form), 28.0, 15.1, 14.3 (enol form), 14.1; HRMS (ESI) calculated for $C_{16}H_{18}O_4$ $[M+H]^+$ 275.1283, found for 275.1283.

Ethyl 2-(3-(but-3-yn-1-yloxy)phenyl)-4-oxo-1,4-dihydroquinoline-6-carboxylate (4). The title compound was prepared by following general procedure. Yield: 53%; Mp 223-229 ^oC; IR (neat): 3300, 3145, 3085, 2987, 1711, 1646, 1581, 1506, 1491, 1266, 1236, 1126, 1042, 841, 792, 758, 711 cm-1; ^1H NMR (600 MHz, DMSO-d_6) δ 11.92 (s, 1H), 8.70 (d, *J*=1.8 Hz, 1H), 8.19 (dd, *J*=1.8, 8.7 Hz, 1H), 7.86 (d, *J*=8.7 Hz, 1H), 7.51 (t, *J*=7.9 Hz, 1H),7.42 (d, *J*=8.6 Hz, 2H), 7.18 (dd, *J*=1.9, 7.8 Hz, 1H), 6.44 (s, 1H), 4.37 (q, *J*=7.0 Hz, 2H), 4.17 (t, *J*=6.2 Hz, 2H), 2.84 (t, *J*=2.5 Hz, 1H), 2.38 (td, *J*=2.5, 7.2 Hz, 2H), 1.95 (quin, *J*=6.6 Hz, 2H), 1.38 (t, *J*=7.1 Hz, 3H); ^{13}C NMR (125 MHz, DMSO-d_6) δ 177.1, 165.8, 159.2, 151.2, 144.1, 135.9, 131.9, 130.7, 127.5, 124.7, 124.6, 120.2, 117.1, 113.9, 108.8, 84.1, 72.2, 66.7, 61.3, 28.2, 15.0, 14.7; HRMS (ESI) *(m/z)*: calculated for $C_{23}H_{21}NO_4$ $[M-H]^-$ 374.1392, found for 374.1390.

1,1,1,2,2,3,3,4,4,5,5,6,6-tridecafluoro-8-(pent-4-yn-1-yloxy)octane. The perfluro-1-octanol (48 μL, 0.218 mmol), pent-4-yn-1-yl 4-methylbenzenesulfonate (52 mg, 0.218 mmol), KOH (600 mg, 10.7 mmol) and TBAI (10 mg, 0.03 mmol) were dissolved in 9:1 THF/H_2O (1 ml), then refluxed for overnight. After removal of THF in vacuo, the solution was extracted with DCM and purified by column chromatography to give liquid product (50 mg, 53%). ^1H NMR (600 MHz, $CDCl_3$) δ 3.72 (t, *J* = 6.9 Hz, 2H), 3.55 (t, *J* = 6.2 Hz, 2H), 2.45-2.34 (m, 2H), 2.31-2.26 (m, 2H), 1.94 (t, *J* = 2.6 Hz, 1H), 1.78 (quint, *J* = 6.7 Hz, 2H), 3.54 (q, *J* = 7.2 Hz, 2H), 1.23 (t, *J* = 7.1 Hz, 3H); ^{13}C NMR (150 MHz, $CDCl_3$) δ 83.6, 69.4, 68.5, 62.7, 31.7, 31.5, 31.4, 28.4, 15.1; ^{19}F NMR (564 MHz, $CDCl_3$) δ -127.2, -124.7, -123.9, -122.9, -114.4, -81.9. HRMS (APCI) *(m/z)*: calculated for $C_{13}H_{12}OF_{13}$ $[(M+H)^+]$ 431.0681, found $[(M+H)^+]$ 431.0682.

Azido-PEG12-MBs. Carboxylated magnetic beads (10 mg) were dispersed into MES (50 mM, pH 6.0, 300 μL). *N*-hydroxysuccinimide (NHS, 3.5 mg, 0.03 mmol) and 1-ethyl-3-(3-dimethylaminopropyl)carbodiimide hydrochloride (EDC· HCl, 5.7 mg, 0.03 mmol) were added to the solution and stirred for 1.5 h at room temperature. The resulting beads were washed with PBS (50 mM, pH 7.0, 300 μL x 2) to remove excess NHS and EDC· HCl. 200 μL of 1 mM carboxylated-

PEG_{12}-amine (pH 7.8 in 50 mM HEPES) was added to the beads and then stirred for 6 hr at room temperature. After separation with a magnet, the beads were washed with MES (50 mM, pH 6.0) to give carboxyl-PEG_{12}-MBs. Carboxyl-PEG_{12}-MBs (10 mg) were dispersed into MES (50 mM, pH 6.0, 300 μL). *N*-hydroxysuccinimide (NHS, 3.5 mg, 0.03 mmol) and 1-ethyl-3-(3 dimethylaminopropyl)carbodiimide hydrochloride (EDC□HCl, 5.7 mg, 0.03 mmol) were added to the solution and stirred for 1.5 h at room temperature. The resulting beads were washed with PBS (50 mM, pH 7.0, 300 μL x 2) to remove excess NHS and EDC□HCl. 200 μL of 1 mM 3-azidopropan-1-amine (pH 7.0 in 50 mM PBS) was added to the beads and then stirred for 16 hr at room temperature. After separation with a magnet, the beads were washed with MES (50 mM, pH 6.0) to give Azido-PEG_{12}-MBs.

Mag-beads-control. To a solution of Azido-PEG_{12}-MBs (10 mg), 1,1,1,2,2,3,3,4,4,5,5,6,6-tridecafluoro-8-(pent-4-yn-1-yloxy)octane (1.72 mg, 4.0 μmol), $CuSO_4$ in 0.1 M dd-H_2O (6.6 μL) and sodium ascorbate in 0.1 M dd-H_2O (1.3 μL) was in *t*-Butanol/dd-H2O (0.3 mL, 1/1, v/v) and in Microwave condition: 100 W, 60°C for 30 min. After separation with a magnet, the beads were washed with MES (50 mM, pH 6.0) to give **Mag-beads-control.**

Mag-beads-AS1712. To a solution of Azido-PEG_{12}-MBs (10 mg), RJ-LC-15-12 (1.5 mg, 4.0 μmol), $CuSO_4$ in 0.1 M dd-H_2O (6.6 μL) and sodium ascorbate in 0.1 M dd-H_2O (1.3 μL) was in *t*-Butanol/dd-H_2O (0.3 mL, 1/1, v/v) and in Microwave condition: 100 W, 60°C for 30 min. After separation with a magnet, the beads were washed with MES (50 mM, pH 6.0) to give **Mag-beads-AS1712.**

Author Contributions

The high-throughput compound library screening was designed and performed by C.H. Wong, P.C. Yang, T.J.R. Cheng, and R.J. Chein; The *in vitro* and *in vivo* experiments were performed by M.S. Lin, S.C. Yang, and W.C. Chung; C.W. Weng and J.J.W. Chen performed the molecular modeling; T.H. Chou, M.L. Tsai, and R.J. Chein performed the chemical structure modification; M.S.

Lin, T.M. Hong, T.H. Chou, C.W. Weng, T.C. Lee, C.H. Wong, R.J. Chein, and P.C. Yang designed the experiments and wrote the manuscript.

Conflicts of interest

The authors declare no competing financial interest.

Acknowledgements

This research was supported by the Ministry of Science and Technology (MOST-106-2314-B-002-103-MY2, MOST-107-0210-01-19-01, 107-2314-B-002-239, MOST-108-3114-Y-001-002) and Academia Sinica (AS-SUMMIT-108). We acknowledged the Light Microscopy Core Facility of the Institute of Biomedical Sciences for their technical assistance; the use of the Biacore T200 in the Biophysics Core Facility, funded by Academia Sinica Core Facility and Innovative Instrument Project (AS-CFII108-111).

Supplementary data

Tumor images, tumor weights, H&E stained sections, body masses, and serum biochemical markers of test mice; time course treatment of AS1712 in CL1-0, H1975, and HFB cells; the effects of AS1712 on HFB cells; the *in vitro* and *in vivo* functional assays of RJ-LC-15-8; ^{1}H, ^{13}C and ^{19}F NMR Spectra and LC Spectra; Modeling of tubulin-AS1712

References

[1] R.L. Siegel, K.D. Miller, A. Jemal, Cancer statistics, 2018, CA Cancer J Clin, 68 (2018) 7-30.
[2] K.S. Nguyen, J.W. Neal, First-line treatment of EGFR-mutant non-small-cell lung cancer: the role of erlotinib and other tyrosine kinase inhibitors, Biologics, 6 (2012) 337-345.
[3] A. Chang, Chemotherapy, chemoresistance and the changing treatment landscape for NSCLC, Lung Cancer, 71 (2011) 3-10.
[4] D.R. Camidge, W. Pao, L.V. Sequist, Acquired resistance to TKIs in solid tumours: learning from lung cancer, Nat Rev Clin Oncol, 11 (2014) 473-481.
[5] F.R. Hirsch, G.V. Scagliotti, J.L. Mulshine, R. Kwon, W.J. Curran, Y.-L. Wu, L. Paz-Ares, Lung cancer: current therapies and new targeted treatments, The Lancet, 389 (2017) 299-311.
[6] A. Desai, T.J. Mitchison, Microtubule polymerization dynamics, Annu Rev Cell Dev Biol, 13 (1997) 83-117.
[7] D. Calligaris, P. Verdier-Pinard, F. Devred, C. Villard, D. Braguer, D. Lafitte, Microtubule targeting agents: from biophysics to proteomics, Cell Mol Life Sci, 67 (2010) 1089-1104.
[8] K. Tanabe, Microtubule Depolymerization by Kinase Inhibitors: Unexpected Findings of Dual Inhibitors, Int J Mol Sci, 18 (2017).
[9] J. Zhou, P. Giannakakou, Targeting microtubules for cancer chemotherapy, Curr Med Chem Anticancer Agents, 5 (2005) 65-71.

[10] Y. Ilan, Microtubules: From understanding their dynamics to using them as potential therapeutic targets, J Cell Physiol, 234 (2019) 7923-7937.
[11] J.M. A., W. L., Microtubules as a target for anticancer drugs, Nat Rev Cancer 4(2004) 253-265.
[12] A. Rovini, A. Savry, D. Braguer, M. Carre, Microtubule-targeted agents: when mitochondria become essential to chemotherapy, Biochim Biophys Acta, 1807 (2011) 679-688.
[13] L. Wilson, D. Panda, M.A. Jordan, Modulation of microtubule dynamics by drugs: a paradigm for the actions of cellular regulators, Cell Struct Funct, 24 (1999) 329-335.
[14] M. Hasanpourghadi, A.K. Pandurangan, M.R. Mustafa, Microtubule Targeting Agents in Cancer Therapy: Elucidating the Underlying Molecular Mechanisms, in: Molecular Oncology: Underlying Mechanisms and Translational Advancements, 2017, pp. 15-65.
[15] Y.N. Cao, L.L. Zheng, D. Wang, X.X. Liang, F. Gao, X.L. Zhou, Recent advances in microtubule-stabilizing agents, Eur J Med Chem, 143 (2018) 806-828.
[16] R. Callaghan, F. Luk, M. Bebawy, Inhibition of the multidrug resistance P-glycoprotein: time for a change of strategy?, Drug Metab Dispos, 42 (2014) 623-631.
[17] G.A. Orr, P. Verdier-Pinard, H. McDaid, S.B. Horwitz, Mechanisms of Taxol resistance related to microtubules, Oncogene, 22 (2003) 7280-7295.
[18] M. Kavallaris, Microtubules and resistance to tubulin-binding agents, Nat Rev Cancer, 10 (2010) 194-204.
[19] P.P. Gan, E. Pasquier, M. Kavallaris, Class III beta-tubulin mediates sensitivity to chemotherapeutic drugs in non small cell lung cancer, Cancer Res, 67 (2007) 9356-9363.
[20] A.J. Chien, M.M. Moasser, Cellular mechanisms of resistance to anthracyclines and taxanes in cancer: intrinsic and acquired, Semin Oncol, 35 (2008) S1-S14; quiz S39.
[21] B.C. Baguley, Multiple drug resistance mechanisms in cancer, Mol Biotechnol, 46 (2010) 308-316.
[22] C. Marquette, L. Nabell, Chemotherapy-resistant metastatic breast cancer, Curr Treat Options Oncol, 13 (2012) 263-275.
[23] K. Katayama, K. Noguchi, Y. Sugimoto, Regulations of P-Glycoprotein/ABCB1/MDR1 in Human Cancer Cells, New Journal of Science, 2014 (2014) 1-10.
[24] W. Li, H. Zhang, Y.G. Assaraf, K. Zhao, X. Xu, J. Xie, D.H. Yang, Z.S. Chen, Overcoming ABC transporter-mediated multidrug resistance: Molecular mechanisms and novel therapeutic drug strategies, Drug Resist Updat, 27 (2016) 14-29.
[25] C.J. Chen, J.E. Chin, K. Ueda, D.P. Clark, I. Pastan, M.M. Gottesman, I.B. Roninson, Internal duplication and homology with bacterial transport proteins in the mdr1 (P-glycoprotein) gene from multidrug-resistant human cells, Cell, 47 (1986) 381-389.
[26] J.A. Endicott, V. Ling, The biochemistry of P-glycoprotein-mediated multidrug resistance, Annu Rev Biochem, 58 (1989) 137-171.
[27] I.S. Mohammad, W. He, L. Yin, Understanding of human ATP binding cassette superfamily and novel multidrug resistance modulators to overcome MDR, Biomed Pharmacother, 100 (2018) 335-348.
[28] W. Li, Y. Shao, L. Hu, X. Zhang, Y. Chen, L. Tong, C. Li, X. Shen, J. Ding, BM6, a new semi-synthetic vinca alkaloid, exhibits its potent in vivo anti-tumor activities via its high binding affinity for tubulin and improved pharmacokinetic profiles, Cancer Biology & Therapy, 6 (2007) 787-794.
[29] B.M. Ibbeson, L. Laraia, E. Alza, O.C. CJ, Y.S. Tan, H.M. Davies, G. McKenzie, A.R. Venkitaraman, D.R. Spring, Diversity-oriented synthesis as a tool for identifying new modulators of mitosis, Nat Commun, 5 (2014) 3155.
[30] R.B. Ravelli, B. Gigant, P.A. Curmi, I. Jourdain, S. Lachkar, A. Sobel, M. Knossow, Insight into tubulin regulation from a complex with colchicine and a stathmin-like domain, Nature, 428 (2004) 198-202.
[31] P.C. Lee, H.J. Lee, R. Kakadiya, K. Sanjiv, T.L. Su, T.C. Lee, Multidrug-resistant cells overexpressing P-glycoprotein are susceptible to DNA crosslinking agents due to attenuated Src/nuclear EGFR cascade-activated DNA repair activity, Oncogene, 32 (2013) 1144-1154.
[32] A. Nadkar, C. Pungaliya, K. Drake, E. Zajac, S.S. Singhal, S. Awasthi, Therapeutic resistance in lung cancer, Expert Opin Drug Metab Toxicol, 2 (2006) 753-777.
[33] G. Borisy, R. Heald, J. Howard, C. Janke, A. Musacchio, E. Nogales, Microtubules: 50 years on from the discovery of tubulin, Nat Rev Mol Cell Biol, 17 (2016) 322-328.

[34] A. Rai, S. Kapoor, A. Naaz, M. Kumar Santra, D. Panda, Enhanced stability of microtubules contributes in the development of colchicine resistance in MCF-7 cells, Biochem Pharmacol, 132 (2017) 38-47.
[35] C. Dumontet, M.A. Jordan, Microtubule-binding agents: a dynamic field of cancer therapeutics, Nat Rev Drug Discov, 9 (2010) 790-803.
[36] K.E. Gascoigne, S.S. Taylor, How do anti-mitotic drugs kill cancer cells?, J Cell Sci, 122 (2009) 2579-2585.
[37] C. Levrier, M.C. Sadowski, A. Rockstroh, B. Gabrielli, M. Kavallaris, M. Lehman, R.A. Davis, C.C. Nelson, 6alpha-Acetoxyanopterine: A Novel Structure Class of Mitotic Inhibitor Disrupting Microtubule Dynamics in Prostate Cancer Cells, Mol Cancer Ther, 16 (2017) 3-15.
[38] Y. Lu, J. Chen, M. Xiao, W. Li, D.D. Miller, An overview of tubulin inhibitors that interact with the colchicine binding site, Pharm Res, 29 (2012) 2943-2971.
[39] A. Dorleans, B. Gigant, R.B. Ravelli, P. Mailliet, V. Mikol, M. Knossow, Variations in the colchicine-binding domain provide insight into the structural switch of tubulin, Proc Natl Acad Sci U S A, 106 (2009) 13775-13779.
[40] S.J. Stafford, J. Schwimer, C.T. Anthony, J.L. Thomson, Y.Z. Wang, E.A. Woltering, Colchicine and 2-methoxyestradiol Inhibit Human Angiogenesis, J Surg Res, 125 (2005) 104-108.
[41] C. Kanthou, G.M. Tozer, Microtubule depolymerizing vascular disrupting agents: novel therapeutic agents for oncology and other pathologies, Int J Exp Pathol, 90 (2009) 284-294.
[42] C. Stengel, S.P. Newman, M.P. Leese, B.V. Potter, M.J. Reed, A. Purohit, Class III beta-tubulin expression and in vitro resistance to microtubule targeting agents, Br J Cancer, 102 (2010) 316-324.
[43] W. Yan, T. Yang, J. Yang, T. Wang, Y. Yu, Y. Wang, Q. Chen, P. Bai, D. Li, H. Ye, Q. Qiu, Y. Zhou, Y. Hu, S. Yang, Y. Wei, W. Li, L. Chen, SKLB060 Reversibly Binds to Colchicine Site of Tubulin and Possesses Efficacy in Multidrug-Resistant Cell Lines, Cell Physiol Biochem, 47 (2018) 489-504.
[44] L. Li, S. Jiang, X. Li, Y. Liu, J. Su, J. Chen, Recent advances in trimethoxyphenyl (TMP) based tubulin inhibitors targeting the colchicine binding site, Eur J Med Chem, 151 (2018) 482-494.
[45] M.M. Gottesman, T. Fojo, S.E. Bates, Multidrug resistance in cancer: role of ATP-dependent transporters, Nat Rev Cancer, 2 (2002) 48-58.
[46] Z. Chen, T. Shi, L. Zhang, P. Zhu, M. Deng, C. Huang, T. Hu, L. Jiang, J. Li, Mammalian drug efflux transporters of the ATP binding cassette (ABC) family in multidrug resistance: A review of the past decade, Cancer Lett, 370 (2016) 153-164.
[47] A. Palmeira, E. Sousa, M.H. Vasconcelos, M.M. Pinto, Three decades of P-gp inhibitors: skimming through several generations and scaffolds, Curr Med Chem, 19 (2012) 1946-2025.
[48] M.L. Amin, P-glycoprotein Inhibition for Optimal Drug Delivery, Drug Target Insights, 7 (2013) 27-34.
[49] E.S. Thomas, H.L. Gomez, R.K. Li, H.C. Chung, L.E. Fein, V.F. Chan, J. Jassem, X.B. Pivot, J.V. Klimovsky, F.H. de Mendoza, B. Xu, M. Campone, G.L. Lerzo, R.A. Peck, P. Mukhopadhyay, L.T. Vahdat, H.H. Roche, Ixabepilone plus capecitabine for metastatic breast cancer progressing after anthracycline and taxane treatment, J Clin Oncol, 25 (2007) 5210-5217.
[50] E. Rivera, J. Lee, A. Davies, Clinical development of ixabepilone and other epothilones in patients with advanced solid tumors, Oncologist, 13 (2008) 1207-1223.
[51] Y.W. Chu, P.C. Yang, S.C. Yang, Y.C. Shyu, M.J. Hendrix, R. Wu, C.W. Wu, Selection of invasive and metastatic subpopulations from a human lung adenocarcinoma cell line, Am J Respir Cell Mol Biol, 17 (1997) 353-360.
[52] G. Wu, D.H. Robertson, C.L. Brooks, 3rd, M. Vieth, Detailed analysis of grid-based molecular docking: A case study of CDOCKER-A CHARMm-based MD docking algorithm, J Comput Chem, 24 (2003) 1549-1562.

Highlights

- AS1712 is active against broad cancer cell lines, even in drug resistant cells.
- AS1712 is a low toxic colchicine-binding site inhibitor.
- RJ-LC-15-8 had a greater anti-proliferative potency with a similar mechanism.
- AS1712 and RJ-LC-15-8 can induce apoptosis in p-gp mediated MDR cells.
- AS1712 and RJ-LC-15-8 have great potential for cancer therapy